Detectability of carbon with ChemCam LIBS: Distinguishing sample from Mars atmospheric carbon, and application to Gale crater

P. Beck [a,b,*], P.Y. Meslin [c], A. Fau [c], O. Forni [c], O. Gasnault [c], J. Lasue [c], A. Cousin [c], S. Schröder [d], S. Maurice [c], W. Rapin [c], R.C. Wiens [e], A.M. Ollila [f], E. Dehouck [g], N. Mangold [h], B. Garcia [i], S. Schwartz [b], W. Goetz [j], N. Lanza [f]

[a] Univ. Grenoble Alpes, CNRS, IPAG, 38000 Grenoble, France
[b] Univ. Grenoble Alpes, CNRS, ISTerre, 38000 Grenoble, France
[c] Institut de Recherche en Astrophysique et Planétologie, Université de Toulouse 3 Paul Sabatier, CNRS, CNES, 31400 Toulouse, France
[d] DLR - Institute of Optical Sensors Systems, Berlin, Germany
[e] EAPS, Purdue University, West Lafayette, IN, USA
[f] Los Alamos National Laboratory, Los Alamos, NM 87545, USA
[g] Universite Claude Bernard Lyon1, LGL-TPE, UMR 5276, CNRS, ENSL, UJM, Villeurbanne F-69622, France
[h] LPG, CNRS, Nantes Université, Université Angers, Le Mans Université, 44322 Nantes, France
[i] IFP Energies Nouvelle, Direction Scientifique, France
[j] Geoscience Center, Department of Geobiology, Georg-August-Universität Göttingen, Göttingen, Germany

ARTICLE INFO

ABSTRACT

Onboard NASA's Curiosity rover, the ChemCam LIBS instrument has provided a wealth of information on the chemistry of rocks within Gale crater. Here, we use ChemCam in order to search for carbonates among the >3500 individual targets analyzed by this instrument. Because the carbon-lines are a combination of signal from the CO_2-rich atmosphere and possible carbon from the targets, we developed a laboratory-based univariate calibration obtained under Mars-like atmosphere. We measured different type of carbon-bearing samples (sediments, coals, carbonates) and their mixture with a basaltic powder. Based on this work, the preferred approach to qualitatively assess carbon under a CO_2-rich atmosphere is to use a ratio to an oxygen line (777 nm) and the estimated limit of detection for carbon in a single LIBS point are found to be of 4.5 wt% and 6.9 wt% for reduced and organic carbon, respectively. Considering carbonate, this LOD correspond to about 50 wt% carbonate in the analyzed volume.

Analysis of data obtained on Mars by ChemCam up to sol 3350 reveals the presence of a correlation between the intensity of carbon and oxygen lines, as observed in the laboratory, confirming that most carbon signal is related to ionization of the atmosphere. Some variability in the carbon signal appears related to the physical state of the atmosphere (density, temperature).

Based on a combined analysis of carbon lines and major element compositions (Ca, Fe, Mg), there was no detection of carbonate in the ChemCam dataset up to sol 3355. Therefore, we conclude that carbonate was not present as a major constituent (>50%) in the ChemCam LIBS targets, and that soils are not enriched in carbon beyond the limit of detection. The dominant salts present are sulfate, chlorides, and the lack of carbonates in Gale, while observed in Jezero, may at least partly be related to a difference in protolith.

1. Introduction

The nature and mass of Mars' carbon reservoirs remain to be precisely assessed. Carbon dioxide is the dominant constituent of Mars' atmosphere and its seasonal condensation as CO_2 ice is a major driver of present-day climate. The Martian atmosphere also contains carbon in the form of CH_4, a molecule that was detected by Earth-based telescopes, from orbit and by in situ observations (Formisano et al., 2004; Mumma et al., 2009; Giuranna et al., 2019; Webster et al., 2015, 2018, 2021), though more recent observation may challenge this detection (Korablev

---

et al., 2019). Beside these volatile species of carbon, refractory carbon in the form of carbonate minerals has been identified on Mars' surface, based on diagnostic absorptions in the near- and shortwave-infrared spectral ranges (Ehlmann et al., 2008). These carbonates are encountered within ancient crustal outcrops and are generally geographically associated with phyllosilicates (Ehlmann et al., 2011; Bultel et al., 2015). Based on the position of the spectral features around 2.3 and 2.5 μm, the composition of these carbonates is expected to be Mg- and/or Fe-rich.

Carbonates were also detected in Martian outcrops by in-situ missions. While carbon abundance was constrained <0.3 wt% in Ares Vallis by Pathfinder APXS (Foley et al., 2003), Fe—Mg carbonates were observed by the Spirit rover at the Columbia Hills of Gusev crater, by a combination of Mossbauer and thermal emission spectroscopy (Morris et al., 2010). Constraints on structural carbonate in Mars soil were provided also by in-situ data from the Curiosity rover as part of NASA's Mars Science Laboratory (MSL) mission which landed in Gale crater in 2012 . While CheMin did not report any observable carbonate, neither in the soil (Blake et al., 2013) nor in the lake sediments within its detection limit of ~1% (Rampe et al., 2020), evidence for both organic as well as inorganic carbon was provided by the SAM instrument. Although in trace amounts, a variety of organic compounds have been detected within fine-grained mudstones by the Evolved Gas Analyzer (EGA) and Gas Chromatography- Mass Spectrometer of the SAM instrument (Sample Analysis at Mars) (Freyssinet et al., 2015, Szopa et al., 2020; Stern et al., 2022; Eigenbrode et al., 2018). Later on, the amount of organic carbon in one of these rocks (mudstone 'Cumberland', Yellowknife Bay, near the landing site) was estimated by the SAM combustion experiment to be of the order of 300 ppm (Stern et al., 2022). In addition, the analysis of soils and bedrock with SAM EGA revealed CO_2 release in a broad temperature range (300–550 °C) which may, at least in parts, come from (oxidized) organic material. A possible explanation for the high-temperature CO_2 release (above 550 °C) is the decrepitation of Mg or Fe-bearing carbonates (Leshin et al., 2013; Sutter et al., 2017). Small amounts of carbonates (up to 3 wt%) were only observed recently by the CheMin instrument based on X-ray diffraction (Thorpe et al., 2022). At the same time, Fe- Mg- bearing carbonates were also identified in-situ by the Perseverance rover in bedrock targets in Jezero crater (Seitah area) using different onboard instruments and techniques (Farley et al., 2022; Wiens et al., 2022; Clavé et al., 2023). These predictions are confirmed from orbital near-infrared observations of this site (Ehlmann et al., 2008; Horgan et al., 2020).

Aboard Curiosity, the ChemCam instrument using the LIBS (laser-induced breakdown spectroscopy) technique has shown great utility in assessing the chemistry of rocks and soils remotely in the close vicinity of the rover (Maurice et al., 2016; Wiens et al., 2015). For LIBS, a laser pulse is focused onto the surface of a sample, where a small plasma is created from the sample material. The light of the plasma is then analyzed and provides information about the elemental composition of the sample. One of the strengths of ChemCam resides in its high spatial resolution (< 1 mm, Maurice et al., 2016), its fast analysis capability at distance of a few meters from the rover and the large number of individual analyses (>935,000 laser shots on >3500 different targets at the time of writing), which allows to fill gaps in between the drill sites. So far, emission lines of 24 elements have been detected on Mars, with important implications for the geochemistry of rocks encountered at Gale crater (see for example Mangold et al., 2019; Rapin et al., 2019; Dehouck et al., 2022). Regarding the dominant constituents of life, hydrogen, oxygen, fluorine, phosphorous and sulfur have all been identified by ChemCam in Gale crater rocks, while carbon, nitrogen, and sulfur have been found as part of molecular/mineral fragments in these rocks by SAM (Freissinet et al., 2015; Stern et al., 2015, 2017, 2018; Eigenbrode et al., 2018).

In this paper we focus on the detectability and search for carbon with ChemCam LIBS. Carbon emission is seen in all Martian LIBS data due to the contribution from the CO_2-dominated atmosphere in the laser-induced plasma. In an earlier work, the detectability of carbon and nitrogen with LIBS under martian conditions was investigated, with a focus on organic compounds (Dequaire et al., 2017). Carbonates were also studied with LIBS in Anderson et al. (2017a) as part of a more general study on salts. We expand the laboratory dataset with macromolecular organic carbon, and further investigate the detectability of inorganic carbon in the form of carbonates. Then, an exploration of the extensive ChemCam dataset up to sol 3355 is described and discussed, searching for possible carbon signatures beyond the usual ChemCam carbon signature that stems from atmospheric CO_2.

2. Laboratory measurements of carbon with LIBS: Samples and methodology

The major challenge for carbon detection with LIBS under Martian conditions is the presence of the CO_2 -dominated atmosphere which contaminates the laser-induced plasma with atmospheric carbon atoms (Ollila et al., 2011, 2013; Anderson et al., 2017a; Dequaire et al., 2017; Schröder et al., 2019). When performing LIBS on solid targets, the produced plasma is composed of elements from the target, but the breakdown of the atmospheric constituents also contributes to the measured signature. The carbon and oxygen emission lines that are measured in LIBS data are thus a combination of signal from the target (if O and/or C bearing) and from the atmosphere. This leads to a carbon signal that is systematically detected in spectra acquired under Martian conditions (Gasnault et al., 2015a, 2015b), while most Martian targets analyzed likely contain carbon below ChemCam's detection limit. We aim here to assess the detectability of carbon and the contribution of atmospheric carbon (and its variability) in ChemCam-like LIBS and therefore studied a combination of C-bearing targets together with a suite of C-free samples in a laboratory approach.

2.1. Samples

2.1.1. Carbon-free end-members
The carbon-free samples we analyze include anhydrous silicates and rocks: a Réunion island basalt, a dunite, and a peridotite from the French Massif Central. In addition, a suite of hydrated or hydroxylated minerals were studied: a synthetic goethite (Beck et al., 2011), a serpentinite from the Chenailler Massif, an obsidian glass, and last, two different types of sulfates (kieserite and schwertmannite). Samples were prepared as raw flat surfaces with the exception of the goethite and sulfates that were prepared as pressed pellets from ground powder (typical grain size <150 μm). This suite of samples was defined as being to some extent representative of some of the mineralogical diversity encountered on Mars, and the list is presented in Table 1.

2.1.2. Carbon-bearing end-members
Two types of carbon-bearing endmembers were used in this study: organic and inorganic. In the case of organic carbon, samples from the Penn State coal sample bank were used, which have the advantage of originating from a large batch of homogenized samples, and to have been widely analyzed for their elemental chemistry. We selected coal as an organic carbon endmember because it is relatively easy to handle, and since it has been used in the past as a structural analogue of extraterrestrial abiotic compounds encountered in meteorites (Quirico et al., 2016). The structure and chemistry of coal is a function of the type of precursor (i.e. which kerogen), as well as of the thermal history of the sample, which leads to chemical and structural modifications, a process called maturation. Because coal samples can have very different absorption properties at 1067 nm (Quirico et al., 2016), i.e. at the wavelength of the ChemCam laser, several samples were chosen in order to span a range of maturities (where maturation is a structural modification induced by burial during geological processes), and therefore a range of absorption coefficients at 1067 nm. Being natural samples, these coals can contain some mineral impurities (quartz or clay

Table 1
List of samples used in this work.

	Sample	Locality	Provider	Preparation
Salts	NaCl	unkn.	Grenoble Museum	Pellet
	Dolomite	Alps	P. Beck collection	Raw and pellet
	Calcite	Alps	P. Beck collection	Raw and pellet
	Siderite	Alps	Grenoble Museum	Raw
	Gypse	unkn.	P. Beck collection	Raw
	Mg-sulfate (heptahydrate)	Synthetic	Commercial	Pellet
	Schwermannite	Spain	A. Fernandez-Martinez	Pellet
Coal	PSOC 1532		Penn State Coal Sample Bank	Pellet
	PSOC 1521		Penn State Coal Sample Bank	Pellet
	PSOC 1552		Penn State Coal Sample Bank	Pellet
	PSOC 1539		Penn State Coal Sample Bank	Pellet
	PSOC 1516		Penn State Coal Sample Bank	Pellet
	PSOC 1540		Penn State Coal Sample Bank	Pellet
	DECS 9	Dietz	Penn State Coal Sample Bank	Pellet
Natural rocks	JSC-Mars 1	Hawaii	Johnson Space Center	Pellet
	Serpentinite		E. Lewin collection	Raw
	Peridotite		E. Lewin collection	Raw
	Basalte	Reunion Island	P. Beck collection	Pellet
	C-rich Schist	Laffrey lake	P. Beck collection	Pellet
	Obsidian	Lipari	P. Beck collection	Pellet
	Sediment 7006	Alps, La Grave	S. Schwartz	Pellet
	Sediment 7007	Alps, Lac du Chambon	S. Schwartz	Pellet
	Sediment 7008	Alps, Verdache	S. Schwartz	Pellet
	Sediment 7010	Alps, Digne	S. Schwartz	Pellet
	Sediment 7012	Alps, Muzelle	S. Schwartz	Pellet
	Sediment 7013	Alps, Embrun	S. Schwartz	Pellet
	Sediment 7014	Alps, La Salce	S. Schwartz	Pellet
	Sediment 7022	Alps, Calibier Path	S. Schwartz	Pellet
	Sediment 7025	Alps, Replatte du Gondran	S. Schwartz	Pellet
Mineral	Monazite		E. Lewin collection	Raw

minerals) whose signature could be present in the LIBS signal.

The inorganic carbon bearing samples that were studied are anhydrous carbonates. Samples of natural (alpine) calcite, dolomite and siderite were used, from a local Museum in Grenoble. The selection of these three carbonates offers the possibility to investigate the behavior of carbon lines for three different chemical matrices (Ca, Ca + Mg, Fe) and therefore assess possible "matrix effects" on carbonate detection. In order to assess the effect of grain size on the detectability, samples of carbonates were sieved to different size fractions (<25 µm, 25–50 µm, 50–100 µm, 100–200 µm), and pressed as pellets. By preparing such samples, we can investigate how the volume density of light scattering events (grain-grain and grain-void interfaces) can impact the LIBS laser coupling and the detectability of carbon. Note that the size of the laser spot diameter of the ChemCam reference instrument at the Institut de Recherche en Astrophysique et Planétologie (IRAP) is close to 500 µm, and that for coarser grains sizes only a single or very few grains are analyzed.

2.1.3. Natural carbon-bearing samples

In order to assess the detectability of carbon in the case of natural mixtures of carbon-free and carbon-bearing materials, a series of terrestrial rocks was analyzed. These samples originate from the French Alps and were collected by S. Schwartz and P. Beck. This suite of samples first includes a carboniferous micaschist that was sampled in the vicinity of Laffrey lake, close to the anthracite mine of La Mure. The rest of these terrestrial rocks are sediments from the paleo-margin that were subducted to different depths during disappearance of the Thetys ocean (Schwartz, 2000, PhD). In order to determine the total organic carbon (TOC) and the mineral carbon (MinC) contents of these rocks, aliquots of these samples were analyzed using the Rock Eval 6 pyrolysis procedure (Behar et al., 2001) at the Institut Français du Pétrole et des Energies Nouvelles (Paris, France).

2.1.4. Carbonaceous chondrite

A carbonaceous chondrite of the CM family was analyzed (ALH 84044) as a pure sample and mixed with basaltic material. This sample was selected since carbonaceous chondrites may be seen as analogues to exogenous dust and meteorites falling on Mars, and have the advantage of being available in sufficient abundance to be analyzed by LIBS (unlike Interplanetary Dust Particles). The chosen sample is a CM chondrite (ALH 84044), whose mineralogy is dominated by Mg and Fe-rich serpentines, together with sulfides. The sample contains a few weight percent of carbon in the form of organic matter and to a lesser extent in the form of carbonates (Alexander et al., 2012). So far metallic and chondritic meteorites have been found in Gale crater (Lasue et al., 2019, 2020; Meslin et al., 2019), but carbonaceous chondrites remain undetected.

2.1.5. Mixtures

Further mixtures of carbon-free and carbon bearing samples were prepared by mixing different materials as grounded powders and pressing them into pellets. To this purpose, a large amount of basalt (200 g) was ground and sieved to grain sizes below 100 µm. This large amount was extensively stirred in order to ensure homogeneity of the powder. Then, aliquots of this powder were used and mixed with different carbon-bearing samples. Two types of coal were selected for the mixtures, representing extremes in terms of maturity of the coal (PSOC 1532, less mature, and PSOC 1521, most mature). These two samples were chosen based on earlier work on the IR properties of coals (Quirico et al., 2016; Phan et al., 2021). Two types of carbonates, calcite and dolomite, were additionally used for mixing with the basalt powder.

In addition to mixtures with basalt, a suite of samples was prepared in which carbon-rich materials were mixed with a Martian regolith simulant (JSC Mars-1, Allen et al., 1998, Moroz et al., 2009). These experiments were intended to assess the impact of possible soil "contamination" on the detectability of carbon, but also the detectability

of a carbon-bearing phase if mixed with martian soils.

As will be discussed in the following, the approach to detect carbon is to use the carbon and oxygen line areas and the C/O line area ratio. An oxygen-free sample was therefore studied (NaCl), as well as its mixtures with basalt.

For all mixture studies, mass fractions were prepared with 1, 2, 5, 10 and 25 wt% of carbon-bearing sample that were mixed respectively with 99, 98, 95, 90 and 75 wt% of basalt. Samples were prepared as pressed pellets. For each sample we typically analyzed three locations, to assess the repeatability of the measurement and the possible spatial heterogeneity of the samples.

2.2. IRAP's ChemCam twin instrument

The ChemCam Mast Unit Engineering Qualification model (MU EQM) combined with the Body Unit engineering model (BU EM) is the replica used in the laboratory at IRAP for calibration purposes (see Rapin et al., 2017). The MU EQM is operated in a climate chamber at −10 °C through a window similar to the Remote Warm Electronic Box (RWEB) setup on Mars. The instrument laser beam and line of sight are directed vertically onto a sample tray placed in a vacuum chamber using an adjustable mirror. It can be filled with a Martian gas simulant to create a plasma in conditions similar to those found at the surface of Mars. The typical distance to the targets in the laboratory is 1.6 m, similar to the distance to the calibration targets on the rover but shorter than a typical distance to a target on Mars (from ~2.2 to ~5 m). Due to the presence of additional optics (folding mirror and Martian chamber entrance window), and due to differences in laser performance, the energy on target achieved in the laboratory (~10 mJ) is slightly lower than usually used on Mars (~14 mJ, Maurice et al., 2016), which compensates for the shorter distance to the target in laboratory measurements (Rapin, 2016). The pulse duration is 6 ns and the beam waist is ~500 μm (assuming a Gaussian profile).

All measurements were performed under a simulated Martian atmosphere (by using a pre-mixed gas simulant containing Mars-like proportions of CO_2, Ar and N_2) at a pressure of 8 mbar, in order to reproduce typical atmospheric conditions occurring on the Martian surface. Each sample was analyzed at usually three locations, and 30 spectra (resulting from 30 laser shots) were acquired, and averaged, for each location.

2.3. Data processing and methodology

2.3.1. Line selection

In Fig. 1, the spectra of several of our mineral endmembers are shown, including carbon-rich (coal, carbonate) and carbon-free samples. In this figure, we focus on the Visible and Infrared (VISIR) part of the spectra that was selected for investigations of the carbon signatures. While ChemCam measures the plasma emission across three wavelength ranges corresponding to three different spectrometers (UV, VIS and VISIR), the reasoning behind focusing on the VISIR part is that the carbon signal was normalized to the strong oxygen line at 777 nm as a probe of the excitation of the Martian atmosphere. Therefore, we focused on carbon-lines present in the same spectrometer as the oxygen 777 nm emission feature which actually is a triplet that is not resolved in ChemCam LIBS data. In Fig. 1 we can observe that the chemical elements detected for the various mineral endmembers when analyzed with LIBS are within expectation (Ca for calcite, Mg and Ca for dolomite, Si, Na, K, Ca, Mg for the basalt). For all samples, emission lines related to carbon are clearly visible. They include emission at around 658 nm partially superimposed by hydrogen emission, 678 nm and 723 nm, and a broad signature around 490–515 nm that is attributed to molecular carbon emission (Swan bands, King, 1948, Fig. 1). The attribution of these lines to carbon can be further confirmed by the experiments performed on the mixtures. In Fig. 2, we can observe their progressive increase in intensity as the amount of coal increases in the mixture with basalt.
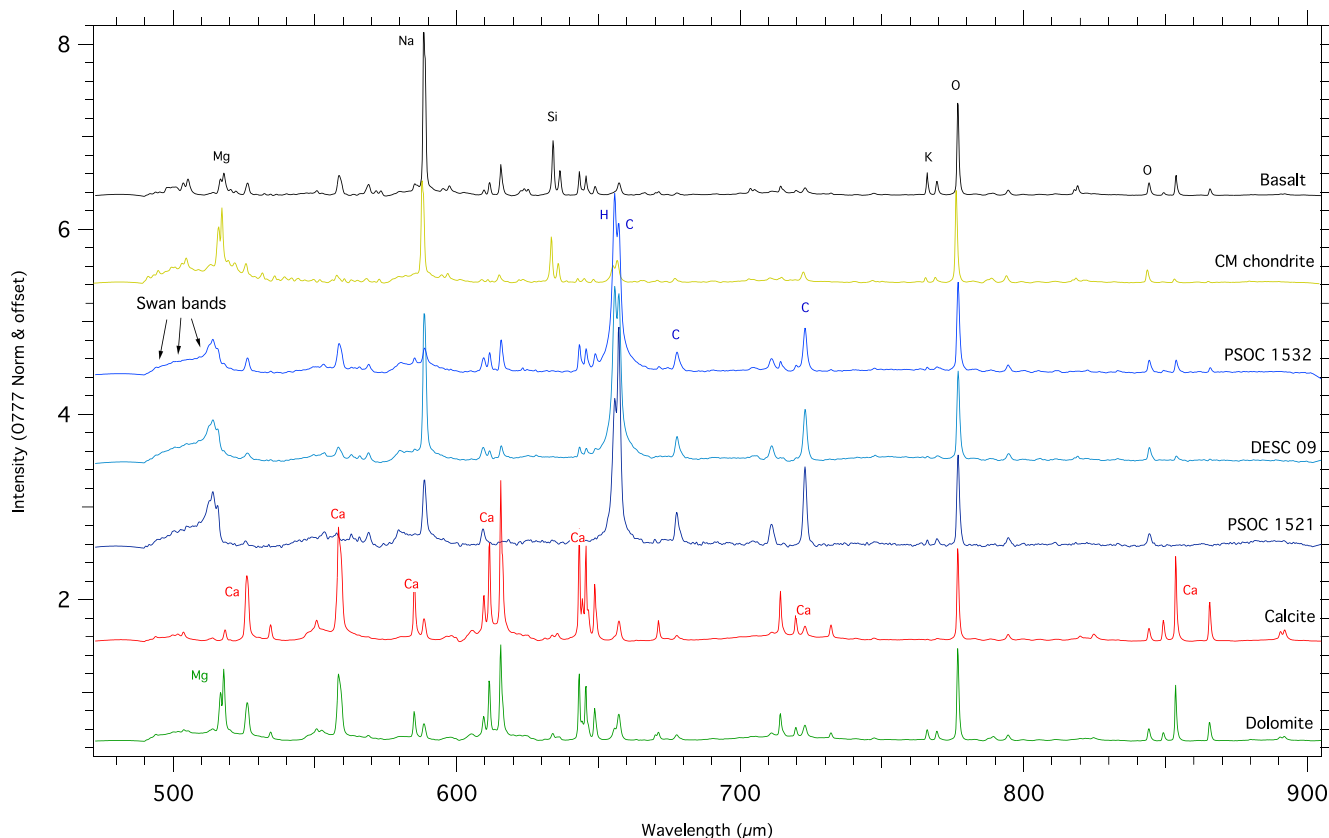

Fig. 1. LIBS spectra across the VISIR spectrometer for different pure end-members used in this study. Emission of selected elements are annotated.
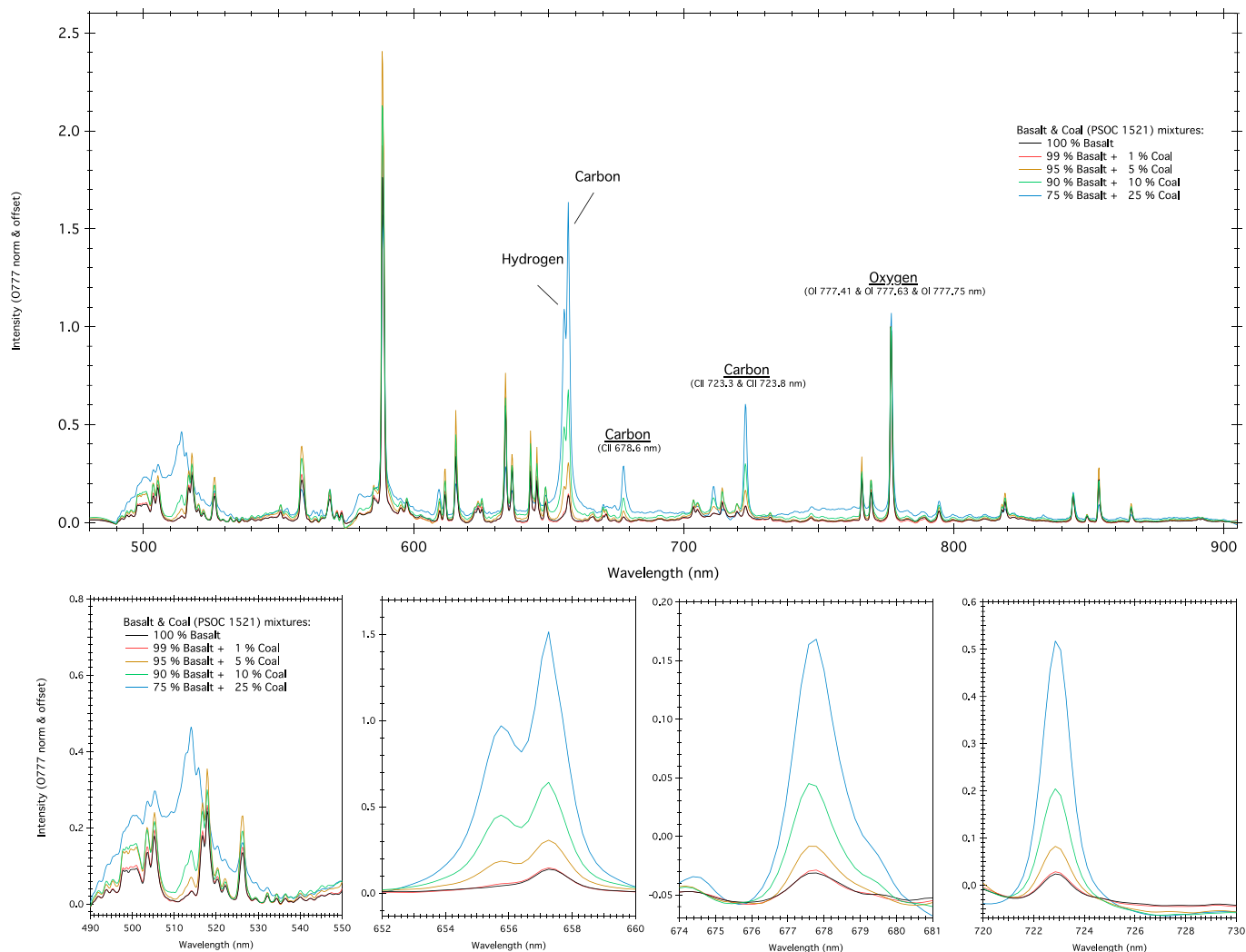
Fig. 2. LIBS data of the basalt-coal mixtures normalized to oxygen emission at 777 nm. The top panel shows the full VISIR spectra, while the bottom panels are focused on carbon-related emissions. In the bottom left panels shows carbon swan bands for the 25 wt% coal bearing mixture. The region around 656 nm corresponds to the superposition of two ionic carbon emission lines which are not resolved in ChemCam LIBS data at approximately 658 nm and the hydrogen emission at 656 nm.

After this first observation step, the two most intense carbon features at 678.6 nm (2 x CII unresolved) and 723.5 nm (CII and CII) were initially investigated and the C678.6 line was selected because it was showing the best detection capability for C (see section 3.4). These two lines were also selected in Anderson et al. (2017a). While the line at 247.9 nm (CI) should be virtually more reliable (since neutral and less sensitive to irradiance), it was not selected given its generally low intensity and the weak correlation of this line intensity with the carbon content of the target possibly due to interferences with iron lines (Schröder et al., 2019). Also, the line at 658 was not analyzed given its proximity to a hydrogen line making its analysis less straightforward. In Fig. 2, the carbon and oxygen peaks used in this study are emphasized.

2.3.2. Combining carbon and oxygen signal to detect carbon

The presence of the CO_2 rich atmosphere makes carbon detection particularly challenging on Mars, since the carbon signal is a combination of carbon from the atmosphere and carbon from the target. Our approach here is to combine LIBS information from both carbon and oxygen. On Mars, the oxygen signal is also a combination of atmospheric and target signal. Indeed, all LIBS spectra obtained on Mars show carbon emission lines and spectra obtained on the oxygen-free Ti target present a strong oxygen signature.

One useful aspect is that dominant minerals encountered on the Martian surface show a relatively narrow variation of oxygen abundance. The fraction of oxygen among major silicates ($NaAlSi_3O_8$, $MgSiO_3$, Mg_2SiO_4, SiO_2) is between 44 wt% to 52 wt%, and this value is similar to that for carbonates (between 41 and 57 wt% for Ca, Fe, Mg carbonate). If we consider bassanite or gypsum (sulfates detected on Mars) the oxygen fraction are 50 wt%. and 56.5 wt% respectively. Therefore, when silicates are analyzed for example, the carbon signal is purely atmospheric while the oxygen signal is the sum of atmospheric signal and target signal. For a similar ablation efficiency and for a stoichiometric ablation, when a carbonate is analyzed the oxygen signal should be of similar magnitude compared to a silicate, while the carbon signal should be higher.

In order to investigate the oxygen signal, the triplet at 777.6 nm was chosen because of the high intensity of this peak and earlier laboratory work (Schröder et al., 2019). Note that the spectral resolution of ChemCam does not resolve the structure of the 777.6 nm oxygen triplet lines (O(I) at 777.41 & 777.63 & 777.75 nm), which is only observed as a single wide line. Similarly, the carbon feature observed at 723.5 nm is in fact a doublet (723.33 and 723.84 nm), which is not resolved.

2.3.3. Line fitting

The selected lines were fitted using pseudo-Voigt functions with the mpfit package available with the IDL software. For each peak, a set of

guess parameters is calculated from the spectrum and used as an input for an efficient fitting. A linear baseline was also adjusted for each peak by using reference points outside of the emission. The typical spectral range where the fit is performed is 4 nm. The quality of the fit was visually inspected for all laboratory spectra. The quality of the fitting process was also verified by calculating fit residuals, and by verifying that the modeled line positions and line widths were correct. Because the oxygen triplet at 777 nm and the C doublet at 723 nm cannot be resolved with ChemCam spectral resolution, these bands were fitted with a single peak.

3. Laboratory measurements: Results

3.1. Carbonaceous chondrites

In Fig. 3, we present the spectra obtained from measuring the mixtures of a basalt and the CM-chondrite, as well as the LIBS spectra of a pure CM chondrite normalized by the triplet oxygen feature at 777 nm. It appears that the intensity of carbon lines is not particularly stronger for the mixture containing 10 wt% of carbonaceous chondrite or less. However, in the case of the pure CM chondrite and the 25 wt% carbonaceous chondrite mixture, the C-lines seem slightly higher than for the

pure basalt (Fig. 3), and carbon from the target is detected. While the name of this class of chondrite is "carbonaceous chondrites", members from this class do not contain more than a few wt% of carbon. In the case of the sample we studied, measurement by Alexander et al. (2012) of another piece of that meteorite gave a value of 1.70 wt% C. We can note that a significant H signal is detected for this sample, in agreement with a phyllosilicate-rich mineralogy (0.703 wt% H or 6.3 wt% H_2O).

3.2. Organic carbon

In Fig. 4 the oxygen 777.6 nm line (O777) area is plotted against the carbon 678.6 nm line (C678) area. On this graph, the measurements obtained for carbon-free samples are shown, as well as the measurements obtained for coal and their mixture with basalt.

First, this graph shows that carbon–free samples define a trend, where the intensities of C678 and O777 are strongly correlated. This correlation can be explained by the fact that as ablation efficiency increases, more atmosphere is excited (increasing carbon and oxygen signal) and more oxygen from the target goes in the plasma (increasing oxygen signal only). It is not possible here to assess the balance between oxygen from the target and oxygen from the atmosphere. The trend defined by C-free samples is not perfect and variability may be related to
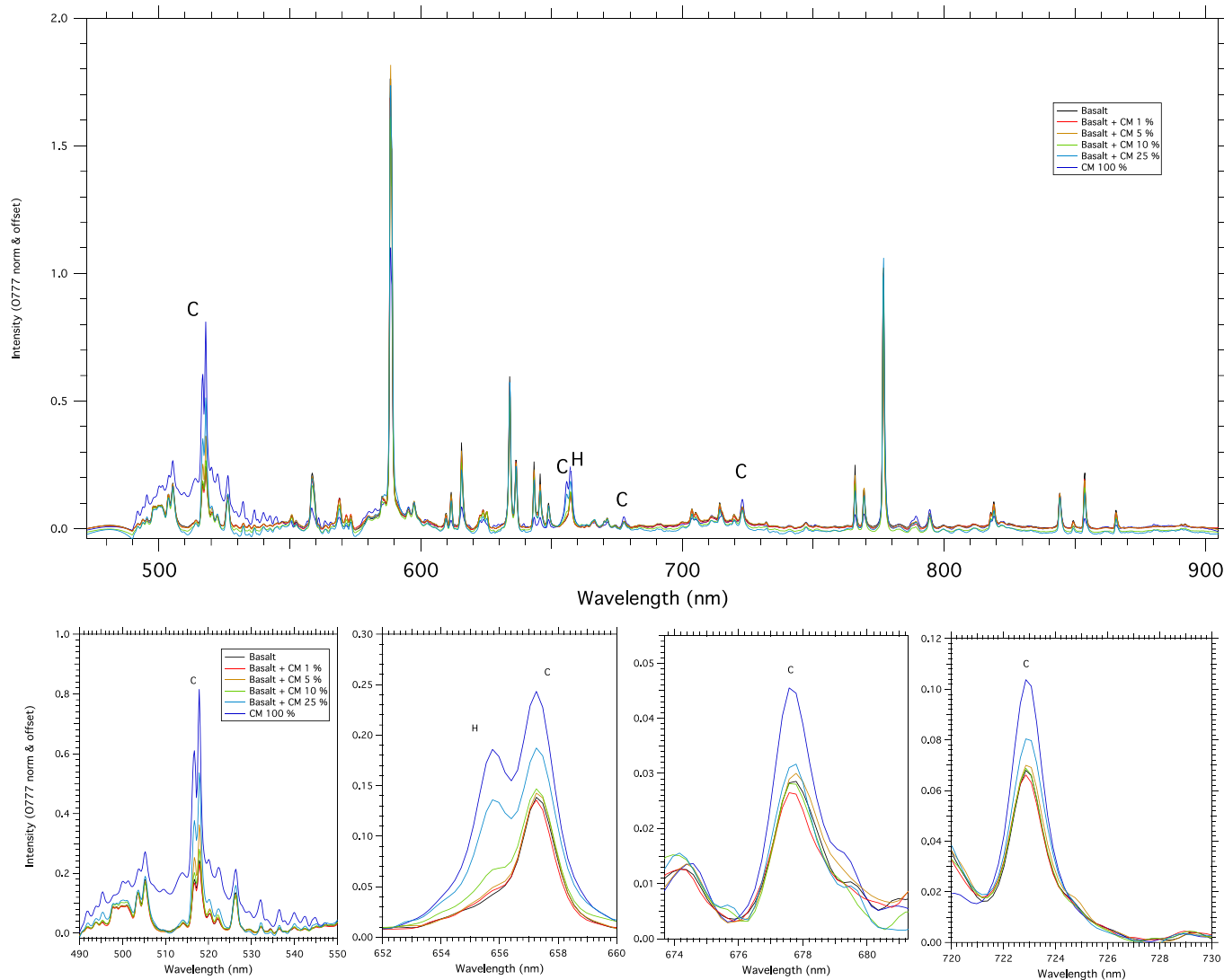

Fig. 3. LIBS data of the basalt-carbonaceous chondrite mixture, normalized to oxygen emission at 777 nm. The top panel shows the full VISIR spectra, while the bottom panels are focused on carbon-related emissions. Note that only for pure CM chondrite are the carbon lines clearly visible in comparison to the spectra of the C-free basalt. Increase of the 656 nm emission is related to the phyllosilicate H_2O content of the CM chondrite sample.
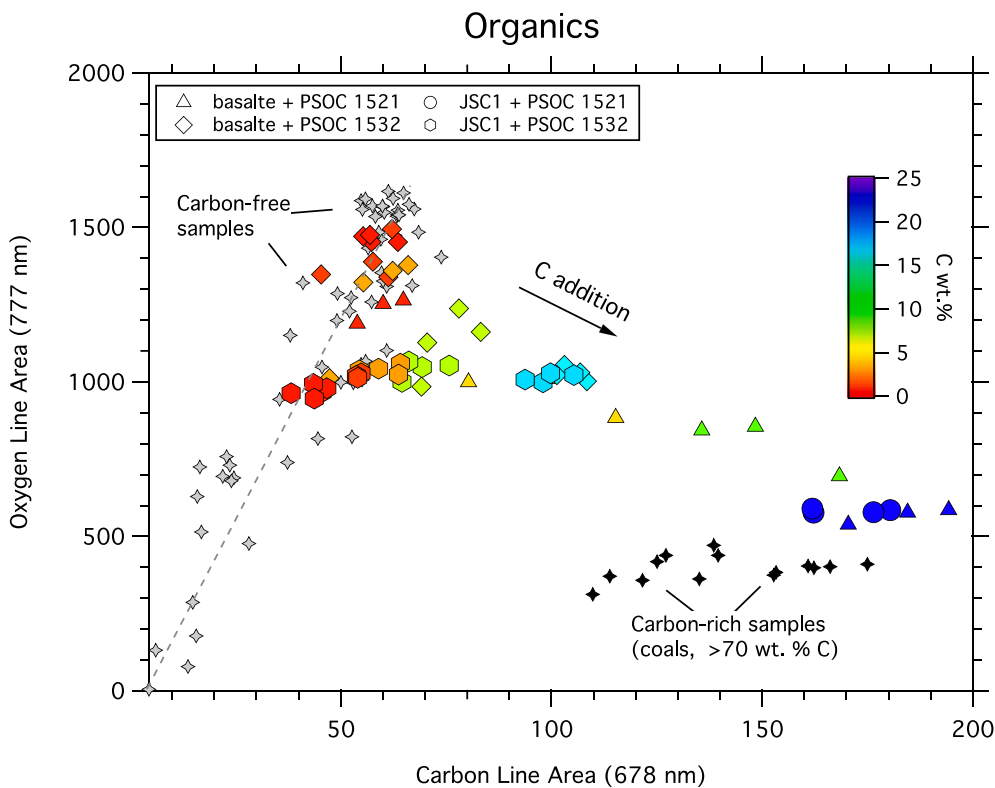
Organics

Fig. 4. Oxygen 777 nm line area as a function of the 678 nm carbon line area, for different organic endmembers and their mixture with basalt and Mars soil analogue (JSC-1).

matrix effects, small variation in the oxygen content of the sample, or non-stoichiometric ablation. We investigated whether the different C-free minerals (silicate, sulfate) define different trends in this diagram, but this was found not to be the case. To further add to the complexity of carbon signal, ChemCam and its twin instrument at IRAP are measuring

the LIBS signal over some duration, that encompasses different stages of the plasma plume (Vogt et al., 2022).

The series of coal measured are clearly located outside of the carbon-free trend and define an almost horizontal trend in this diagram (black symbols on Fig. 4). The data obtained on mixtures between basalt and
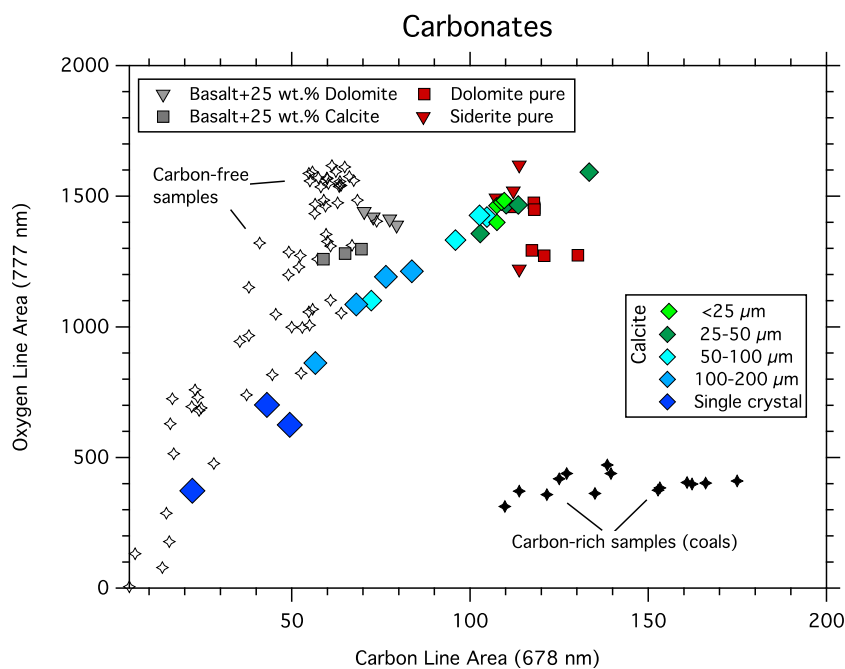
Carbonates

Fig. 5. Oxygen 777 nm line area as a function of the 678 nm carbon line area, for carbonates and their mixture with basalt, as well as the coal samples. This graph also shows the spectra obtained on calcite pellet made out of different grain sizes. The carbonates define a trend slightly offset from the C-free samples. Both C and O area are smaller for coarser grained samples, probably because of worse laser coupling to the sample.

coal fall on a trend that extends from the carbon-free trend to the carbon-rich samples. Measurements obtained for mixtures with carbon concentrations above 5 wt% are located clearly outside of the carbon-free trend, suggesting that in the case of organic carbon, concentrations above 5 wt% C should be readily detected with LIBS under Martian conditions. Note that the low CO_2 abundance under Earth-like conditions makes detection of carbon with LIBS easier in that environment (Dequaire et al., 2017).

3.3. Carbonates

The results obtained for carbonates are shown in Fig. 5 in the plots of O777 vs C678 line areas. This figure shows that pure carbonates define a trend with a lower slope than C-free samples, in other words with a higher C678/O777 line area ratio. This suggests at first order that pure carbonates may be detected with LIBS under Martian conditions (at least the 3 types of carbonates studied here) and could be recognizable in ChemCam data if present as pure phases. More quantitative assessment will be provided in section 3.5.

Carbonates were prepared as a single pressed-pellet for each type, with the exception of calcite, where the impact of grain size was assessed by performing LIBS measurements on a single crystal as well as on pellets pressed from powders with different grain sizes (and therefore different volume densities). The results (Fig. 5) show that the higher the grain size the lower the intensities of the carbon emission features in the LIBS data which can be explained by less good coupling between the laser and the sample. Nevertheless, independently of grain size, all samples fall on a roughly linear trend, distinct from the C-free trend.

In the case of 25 wt% carbonates mixed with 75 wt% basalt, the measurements overlap with the carbon-free samples. These results emphasize the difficulty to detect carbonates under Martian conditions with LIBS, based on a univariate approach with the carbon and the oxygen emission lines. Note that pure carbonates only contain about 12 wt% of carbon (in the case of calcite and dolomite) and that the 25 wt% carbonates - 75 wt% basalt mixtures therefore only contains 3 wt% of carbon.

3.4. Alpine sediments

Results obtained for the alpine sediments are presented in Fig. 6. Samples with the lowest carbon content appear to fall within the carbon-free trend, but samples for which the carbon content was determined to be above 5 wt% are significantly offset from the trend defined by carbon-free samples. For almost all these natural samples, the carbon budget is dominated by carbonates of unknown mineralogy as determined by the Rock Eval 6 analysis. The behavior observed for artificial carbon-bearing mixtures (sections 3.2 and 3.3) is therefore similar to the one observed for natural carbon-bearing rocks.

3.5. Calibration curves and LODs

Our goal is to distinguish the carbon signal coming from the target, from the carbon signal coming from atmospheric CO_2 breakdown. For that, the ratio of the O777 to C678 lines was used, based on our laboratory measurements. In Fig. 7 this ratio is plotted against the carbon content of the analyzed samples. In this diagram, two trends are distinguished. A first trend is defined by samples that are mixtures with PSOC 1521 coal. These are the basalt - PSOC 1521 mixture (1,2,5,10, 25 wt%) and the JSC Mars-1-PSOC 1521 mixture (where only one mixing ratio was studied, 25 wt% PSOC 1521–75 wt% basalt). All other samples define a second trend, with a lower slope than the first trend. The reason for these two separate trends is not fully understood at present. Sample PSOC 1521 is the most mature coal of all samples studied. It is also the poorest in oxygen (O/C atomic ratio = 0.024), and has a lower moisture content. This lack of oxygen may explain the presence of a separate and steeper trend. Another explanation could be related to its different laser absorption properties given its high-maturity. While all coals are dark in the visible, only mature coals have a high absorption coefficient around 1 μm (Quirico et al., 2016). In any case, this suggests that matrix effect may be at play for carbon and non-univariate methods may need to be investigated further.

From these two calibration trends, limits of detection (LOD) for single point measurements were estimated using the 97.5% prediction
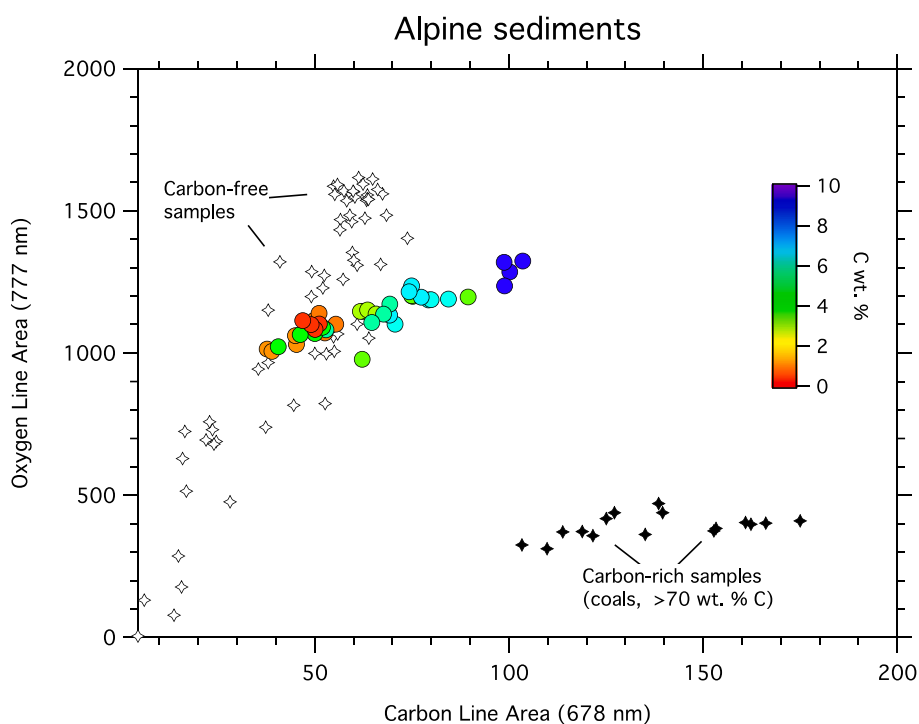

Fig. 6. Oxygen 777 nm line area as a function of the 678 nm carbon line area for the alpine sedimentary rocks. The color code is according to the total carbon abundance (organic+inorganic) derived from RockEval analysis (see main text for more details).
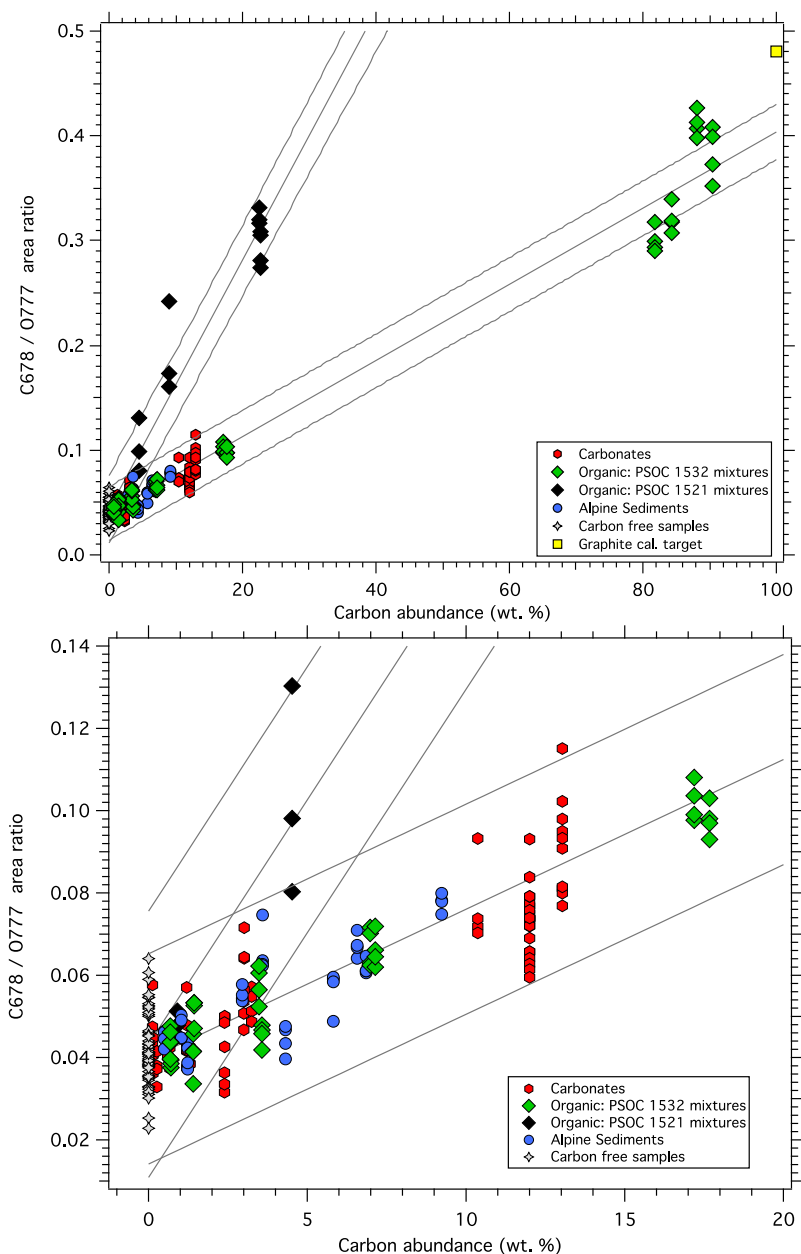
Fig. 7. C678/O777 line area ratio as a function of carbon abundance for the different sample studied. The lines represent the linear regression and the prediction intervals (97.5%).

interval of the linear regression and were found to be of 5 wt% C (for the first trend, mixtures with PSOC 1521) and 13 wt% C (for the second trend, mixtures with oxidized carbon) at the 97.5% confidence level (i. e., the risk of false negatives and false positives is 2.5%). If we calculate the critical level (Lc) of detection (Currie, 1968), defined here for a risk of false positives of 5%, from the C678/O777 line area ratio of C-free samples (average+1.64σ), the L_C values found are 4.5 wt% for reduced carbon and 6.85 wt% for organic carbon. The LOD and L_C are given for single point measurements because the likelihood of detecting carbonates or other carbon-bearing compounds over several adjacent LIBS points on Mars (e.g., in carbonate-rich rocks) is considered less likely than hitting a single mineral at the LIBS scale, especially at low bulk abundances of carbon.

While we use a univariate approach in this study, alternative methods should be tested and used in the future to try to improve the limit of detection or provide independent approaches to confirm carbon detection. In particular the use of supervised or unsupervised

classification methods has shown great performances in the analysis of terrestrial rocks (Chen et al., 2020) and for planetary exploration even when distance to target varies significantly (Yang et al., 2022).

The detection limits we obtained here are higher (and then worse) than the values found by Anderson et al. (2017a, 2017b) in which a 2 wt % LOD was estimated for carbon. This is likely related to their different approach, that only looks at the intensity of the carbon-lines in a binary mixture, and therefore does not take into account variability in their intensity with efficiency of laser coupling (variable on Mars), distance to targets, atmospheric state, which all need to be taken into account when looking at Mars LIBS data. This is why, we designed an approach based on coupled carbon and oxygen lines, that will be applied to Mars in the next section.

4. Applications to Mars LIBS data

ChemCam is a LIBS instrument that enables to determine major and

minor element abundances in the vicinity of the Curiosity rover. Typically, LIBS data are acquired in the form of a "raster", where usually 5 to 10 locations on a target are analyzed with 30 consecutive 10–14 mJ laser shots. The size of the area that is analyzed is in the range of 300 to 550 μm for bedrock targets (Maurice et al., 2016). The LIBS is coupled to a Remote Mast Imager (RMI, Gasnault et al., 2017) providing imaging of the geological context and exact location of the LIBS spots.

4.1. The carbon and oxygen line areas in LIBS spectra of Martian targets

In Fig. 8, the intensity of the O777 line is plotted as a function of the C678 line for data obtained by ChemCam at Gale Crater, Mars. This graph includes all ChemCam targets (soil and rocks) as well as the measurements obtained on the on-board graphite calibration target, from the beginning of the mission to sol 3355 (January 2022). Interestingly, this graph is reminiscent of the results obtained in the laboratory using ChemCam's twin instrument at IRAP. The Martian targets define a trend of correlated increase in the O777 and C678 lines and a similar behavior is observed with the C723 carbon line. This trend implies that these two carbon lines are impacted by contribution from the atmosphere, and the location of a given analysis on this correlation trend may be related to variability in coupling efficiencies and excitation of the atmosphere. The data obtained for the graphite calibration target define a trend with a much lower slope (and therefore higher C/O ratio) in agreement with laboratory results obtained on coal (Fig. 4).

In Fig. 8, the points are color-coded according to the distance to target, which reveals that some of the variability observed in this diagram is due to a distance effect. The targets analyzed closer to ChemCam's telescope tend to have a high (C678/O777), while the targets analyzed further away tend to have a lower (C678/0777). The effect of target distance on the oxygen line and overall LIBS signal was described in Mezzacappa et al. (2014). Because the carbonlines we use are ionized (CII with an ionization energy of 24.38 eV) and the oxygen line is neutral (OI, ionization energy of 13.62 eV), the line intensity ratio should be

sensitive to plasma temperature, that itself may be related to laser irradiance on the target. This provides an explanation for the decay of the C678/O777 ratio with distance to target since laser irradiance decreases with distance (Maurice et al., 2012). Because the (C678/O777) ratio will be used to detect and estimate carbon content based on laboratory results (i.e. Fig. 7), the effect of target distance on C678/O777 needs to be considered when building a carbon detection method. In Fig. 8, several points are located outside of the general trends. These points were explored further individually, but an analysis of their major element chemistry (in particular Major-element Oxide Composition (MOC) totals) ruled out the presence of carbon in the sample, suggesting these points are false detections (see further discussion in 4.3)

4.2. Transferring laboratory results to Mars data

Results obtained in the laboratory cannot be directly transferred to data obtained on Mars by ChemCam. This is due to the fact that the twin instrument in the laboratory is not strictly identical to ChemCam flight model on Mars, and the distance to the targets analyzed with the testbed is fixed while on Mars, targets are analyzed in distances of 2.2 to 5 m. In order to transfer laboratory results to Mars, one can use the fact that both carbon-free and carbon-rich targets were analyzed both in the laboratory and on Mars. In laboratory data obtained here, the C678/O777 ratio derived for graphite is 12.2 times higher than that of carbon-free samples. In the martian dataset, the C678/O777 ratio derived for the graphite calibration target is 11.5 times higher than that derived for the other calibration targets (carbon-free). Because those ratios are similar, we can propose to transpose the laboratory calibration obtained on Earth to the Martian dataset. However, the laboratory-based calibration curves cannot be directly transferred to Martian conditions since the absolute values (C678/O777) are different between Earth and Mars for the C-free trend. The approach we pursued is to make a rough approximation that the (C678/O777) ratio is linearly correlated with the carbon content. This hypothesis surely underestimates the influence of
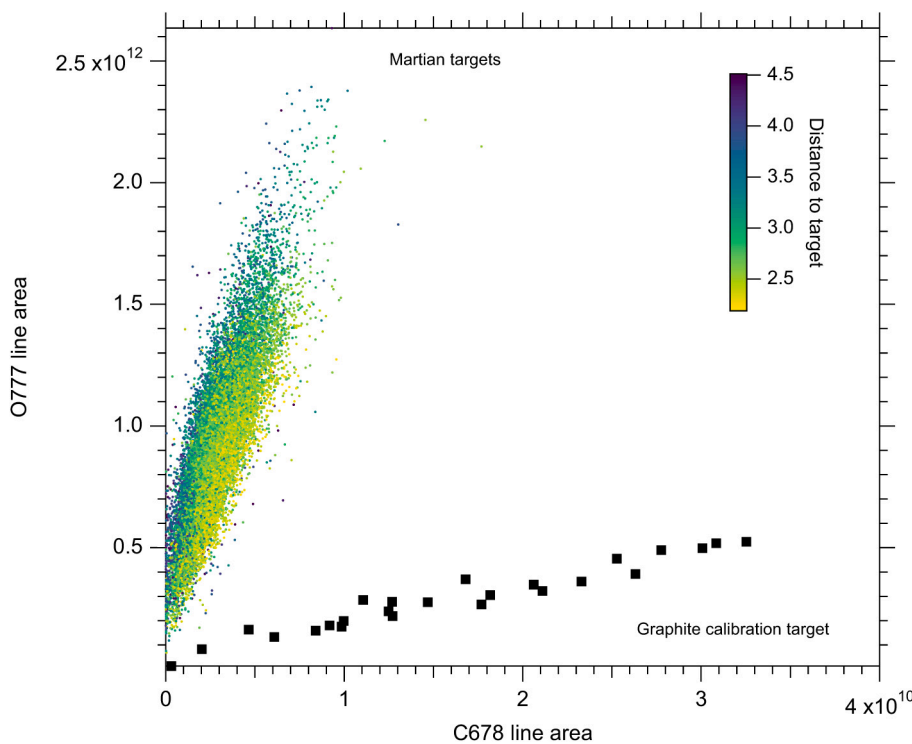

Fig. 8. Oxygen 777 nm line area as a function of the 678 nm carbon line area for data acquired on Mars by ChemCam up to sol 3350. A trend of increasing oxygen and carbon line area is observed, similarly to laboratory data. Results obtained on the pure graphite calibration target are also shown. Note that values are here expressed in radiance, while expressed in arbitrary units in Fig. 4-6.

the effects of varying experimental conditions on Mars as well as of general matrix effects, but is motivated by laboratory data. If we consider ∝ as the slope of the linear relation between carbon content and C678/O777 (Fig. 7) then:

$$\left(\frac{C678}{0777}\right)_{Target} = [C\ wt.\%]_{Target} * \propto + \left(\frac{C678}{0777}\right)_{Carbon-free} \quad (1)$$

and then:

$$[C\ wt.\%]_{Target} = \frac{\left(\frac{C678}{0777}\right)_{Target} - \left(\frac{C678}{0777}\right)_{Carbon-free}}{\propto} \quad (2)$$

The value of alpha can be determined for laboratory data, but this value cannot be used for Martian data because of uncertainly in the Earth to Mars transfer function. Therefore, the value of ∝ is calculated using solely data obtained on Mars on a C-pure target (graphite, [C] = 100 wt%) and carbon-free calibration targets, (see Wiens et al., 2012, Fabre et al., 2011, and Vaniman et al., 2012 for a description of the calibration targets). Then the value is found to be ∝=5.11 × 10^{-4}. By design, the onboard calibration targets of ChemCam can only be measured at a single distance (1.57 m) for which this value of ∝ is derived; we cannot determine ∝ at different distances on Mars.

Because $\left(\frac{C678}{0777}\right)_{Carbon-free}$ depends on the target distance (Figs. 8-9) the ChemCam dataset was binned as a function of distance, and for each range of distances the average (C678/O777) was calculated as well as its standard deviation (Fig. 9). This set of values was taken as our carbon-free reference $\left(\frac{C678}{0777}\right)_{Carbon-free}$ to be used in eq. 2. This approach assumes that the typical targets analyzed by ChemCam are dominated by carbon free targets, which is a very reasonable hypothesis given the results obtained by the SAM and CheMin experiments.

4.3. Lack of carbonates up to sol 3355

In order to assess whether carbonates could be present within the suite of rocks and soils analyzed by ChemCam, the (C678/O777) analysis described above was coupled to the MOC computed from ChemCam data (Wiens et al., 2013; Clegg et al., 2017; Anderson et al., 2017b). In Fig. 10, MOC values for CaO, MgO and FeO$_T$ (total iron as FeO) were plotted as a function of the (C678/O777) line area ratio.

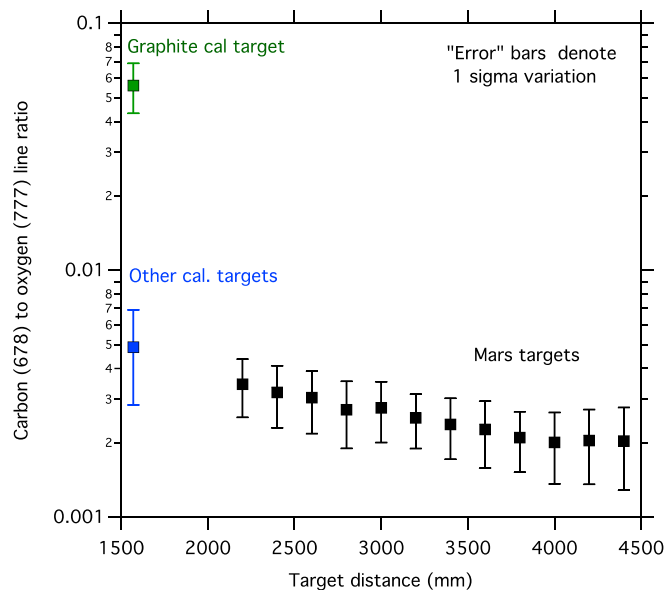In these graphs, the predicted location of carbonates is shown for

Fig. 9. Effect of target distance on the C678 to O777 line area ratio for Martian rock targets, and ChemCam calibration targets.
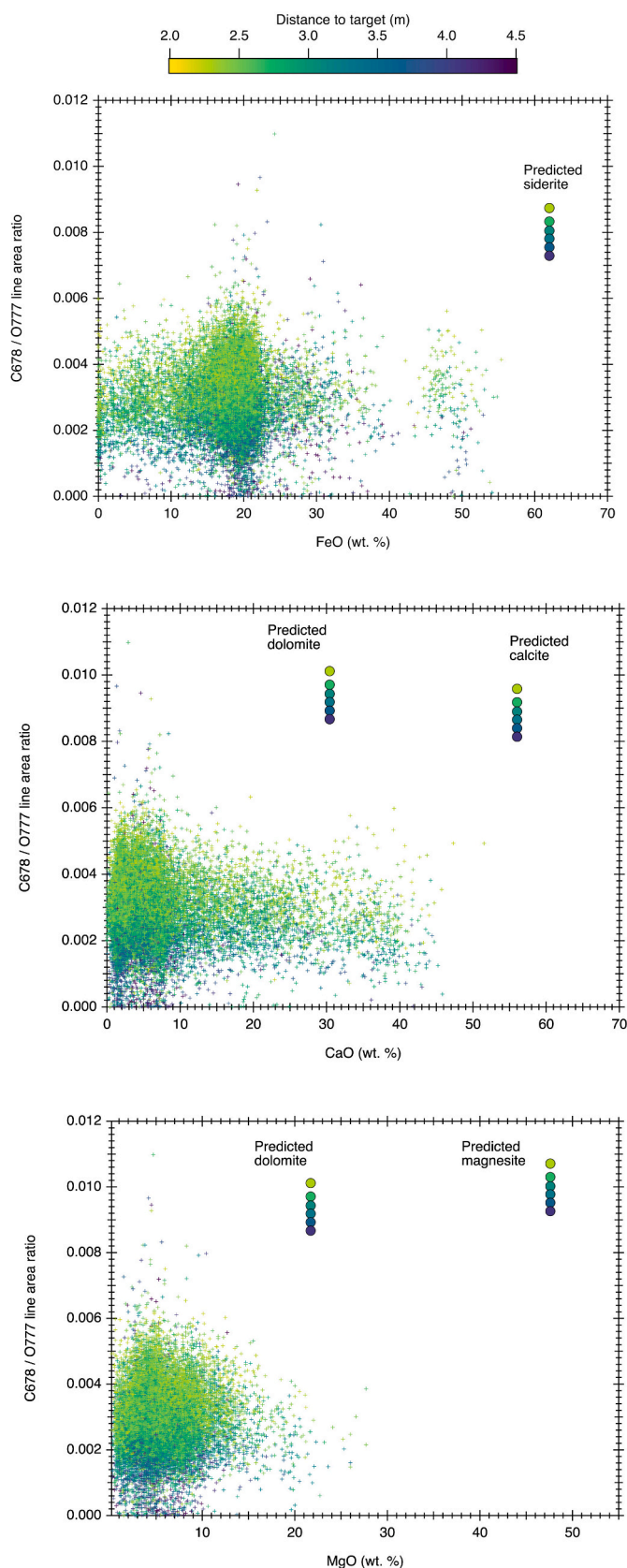

Fig. 10. The C678/O777 line area ratio as a function of different oxide abundances. The location of the predicted position of pure carbonate is also shown. Data are color-coded as a function of the distance to target.

calcite, dolomite, magnesite and siderite, that was obtained using eq. (1). For that we use the carbon content in each of those (in wt%) based on the structural formula ($CaCO_3$, $CaMg(CO_3)_2$, $MgCO_3$, $FeCO_3$), the value of alpha we obtained by comparing carbon signal between the graphite and carbon-free calibration targets (see previous section), and last the (C678/O777) of carbon-free Martian targets. Because the (C678/O777) of carbon-free Martian targets depends on the distance to target, we plot in Fig. 10 the expected location of these carbonates if they were analyzed at different distances, by using (C678/O777) obtained for distance bins within the Martian dataset.

It is clear from this graph that there is no pure carbonate analysis within this dataset, nor are there any strong trends toward one of these carbonate endmembers. A few points show an elevated FeO_T together with a high C678/O777 ratio, however these are interpreted to be Fe-meteorites (based on texture and Ni abundance, Meslin et al., 2019), for which the depletion in oxygen explains the high C678/O777 ratio.

Our results suggest that there were no pure phase carbonates detected by ChemCam at the ~300–500 μm scale. Based on Fig. 10, we can also estimate that there was not more than ~50% carbonate in any of the targets analyzed by ChemCam. These constraints are not as strong as those derived for instance by CheMin analysis (< 1 wt%). However, given the number of analyses performed by ChemCam and the small volume analyzed by LIBS, the presence of carbonates as a cement would produce a trend toward a carbonate endmember in Fig. 10 which is not observed. The major cement that appears to be present is rather Ca-sulfate (Rapin et al., 2016), which explains the horizontal trend seen in the (C678/O777) vs CaO plot (Fig. 10). The lack of carbonates in the ChemCam dataset is in agreement with orbital CRISM observations in this region (Ehlmann and Buz, 2015).

Based on ChemMin X-ray diffraction data, carbonates were only identified relatively recently within the Glen Torridon location (Thorpe et al., 2022). These carbonates are present in minute amounts (1–3 wt%) and are likely Fe-rich. Investigation of ChemCam data failed to detect these carbonates, confirming that they are present in minor amounts, and probably absent in the form of large grains or veins.

4.4. Soils vs rocks: Any exogenous carbon signature?

Models of exogenous carbon flux to Mars clearly predict that there is a non-negligible input of organic-containing extra-terrestrial matter (Quirico and Bonal, 2019). The accretion rate of meteoritic carbon on Mars has been estimated to be around $2.4.10^5$ kg/year (Flynn, 1996; Steininger et al., 2012), which converts into 1.7 kg of carbon per Gy and per square meter. The present-day amount of carbon in the martian soils depends on the soil production rates (mechanical or chemical erosion) and destruction rate (by UV irradiation for instance). The present-day amount of carbon also depends on the chemical processes that specifically remove carbon from the soil: fragmentation of large molecules by irradiation (UV photon, solar wind and galactic cosmic rays) (Quirico and Bonal, 2019; Goetz et al., 2016) and oxidation of reduced carbon (for example by chemical interaction with perchlorates).

In Fig. 11, the (C678/O777) line area ratio is presented as a function of distance to target, for "standard" ChemCam targets as well as for soil targets (including data only up to sol 1550). Soils were studied by ChemCam at different locations, and analyzed at different distances (Cousin et al., 2015). This figure shows that there is no strong difference between soil analyses and other ChemCam targets. The average (C678/O777) values are $(334 +/- 7) \bullet 10^{-5}$ and $(286 +/- 4) \bullet 10^{-5}$ for soil targets and other targets, respectively, where the given uncertainties are the standard errors of the mean. The averages are therefore statistically distinct and this is due to the high (C678/O777) value of several targets analyzed at random location referred to as bling targets. This difference could be due to an enrichment in carbon of the soil targets; but given the variability that was found in (C678/O777) values within laboratory data obtained on carbon-free samples with different matrices, there is no definite evidence for carbon enrichment in martian soils at the detection limit of ChemCam. This is generally in agreement with the lack of carbonate detection in ChemCam rock targets from which soil should be at least partially derived. It is also in agreement with the lack of carbonate detection in the two eolian sediment samples analyzed by CheMin (Achilles et al., 2017).
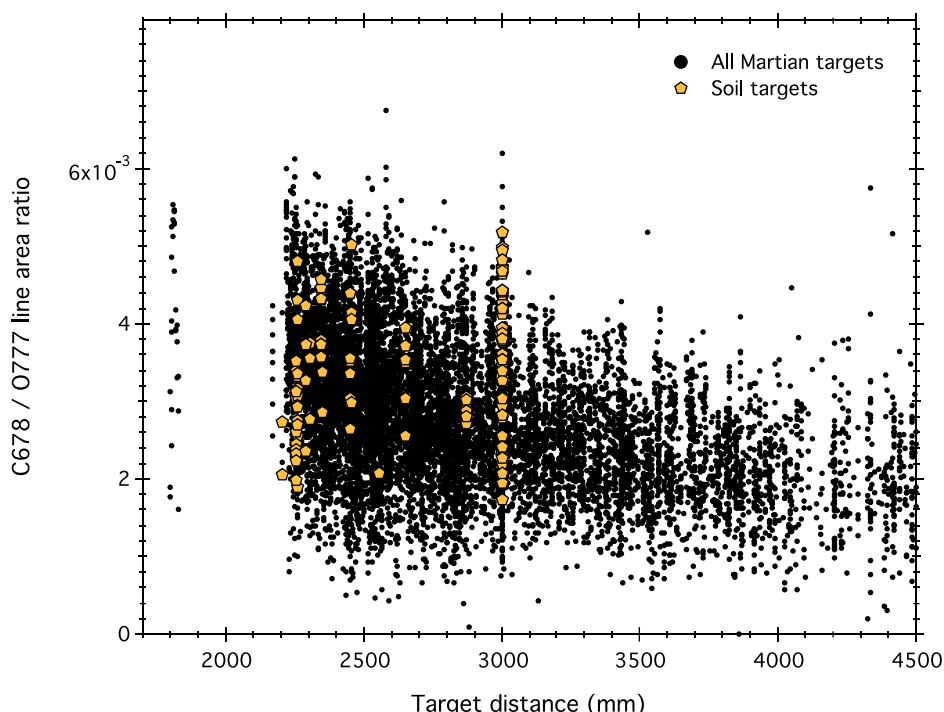

Fig. 11. C678/O777 for all data obtained on Martian targets up to sol 1555 and comparison to data obtained on soil targets.

4.5. Atmospheric effects on the carbon line

In Fig. 12, the variability of the C678/O777 line area ratio is shown as a function of sol since landing of *Curiosity*. Note that on this graph, only LIBS spectra with a total intensity above 2.10^{14} (photons/shot/cm^2/Sr/nm) were selected. This filtering was applied in order to remove from our dataset targets for which the quality of coupling was likely poor (bad focus). Also, data obtained on calibration targets are not included since acquired at a distance much shorter than Martian targets, and only

targets measured at a distance lower than 4.5 m were selected.

Typical Martian targets have a C678/O777 ratio around 0.004, but some variability is seen across the transect. Four maxima appear to be present around sols 700 and 1400, 2100 and 2800 which are separated by about one Martian year. In order to assess possible relation between the C678/O777 ratio and the physical state of the atmosphere, we used surface temperature, atmospheric pressure and density at Gale crater derived from the Mars Climate Database (Forget et al., 1999; Millour et al., 2018) (Fig. 12). Values of these parameters were calculated at

Fig. 12. Seasonal behavior of the C/O ratio. The panels on the left side are shown according to sol to landing (thus showing several martian years one after the other), while the panels are the right are "wrapped" thus superimposing several martian years. The top right panel also indicates the corresponding subsolar longitude values. The points are the individual ChemCam analysis. Data obtained only between 2 and 3 m are shown to minimize variation induced by distance to target. The various curves were calculated using the Mars Climate Database (Forget et al., 1999; Millour et al., 2018).

noon, typical time of ChemCam observation. As can be seen in Fig. 12, the maxima in C678/O777 seem to correspond to maxima in surface temperature, and minima in atmospheric density. Such variations in temperature are too low to produce an effect on the plasma condition, but the variations in density are significant and may explain a seasonal behavior.

In order to confirm the presence of a dependence to atmospheric conditions, we used the variation of the C678/O777 ratio with local mean solar time (LMST), and take benefit of the presence of rare but useful measurements perform in the early morning. It can be observed (Fig. 13) that in the early morning observations, corresponding to a cold and dense atmosphere, the C678/O777 ratio is significantly lower than during more typical observations (around noon). This behavior is therefore consistent with the seasonal evolution we observed (Fig. 12). While these effects may be related to the physics of plasma production in relation to the thermodynamical state of the atmosphere, we cannot rule out an effect related to instrumental performance at variable temperature.

4.6. Jezero vs Gale: Sulfates vs carbonates

Unlike Gale crater, carbonate-bearing deposits have been detected within Jezero crater from orbital observations (Ehlmann et al., 2008; Horgan et al., 2020). Relatively soon after landing, *Perseverance* investigations of geological units from the igneous crater floor confirmed the presence of carbonates in some of the bedrock targets (Wiens et al., 2022; Farley et al., 2022). The SuperCam instrument (Maurice et al., 2021; Wiens et al., 2021), with a strong heritage from ChemCam, was able to detect Fe—Mg carbonates by combining LIBS, VISIR spectroscopy and Raman spectroscopy (Clavé et al., 2023). These carbonates are intimately associated to mafic minerals (in particular olivines), and were possibly formed during hydrothermal alteration of the igneous protolith at relatively low water-rock ratio (Clavé et al., 2023).

In order to assist with carbonate detections, the *Perseverance* rover also hosts calcite, ankerite, and siderite calibration targets on its deck, among other SuperCam Calibration Targets (SCCTs, Manrique et al., 2020, Cousin et al., 2022). Analysis of these targets revealed C- vs O-line correlations (Clavé et al., 2023) as well a target distance effect on C678/O777 ratio determined on martian targets, similar to our observations for ChemCam. The presence of the carbonate targets provides additional grounds for carbon quantification. The C678/O777 area ratio for C-poor calibration targets is around 0.011, while it is around 0.019 for the calcite calibration target. This increase by roughly a factor of two in the C678/O777 in the calcite SCCT compared to other SCCTs is in agreement with the increase observed here in the laboratory for carbonates compared to carbon-free samples (Fig. 7).

The confirmed detection with a similar instrument in another location on Mars (Clavé et al., 2023) suggests that ChemCam could have detected carbonates if there were enough in the targets reported here for Gale crater.

While carbonates were observed in ultramafic rock of Jezero crater, including as veins (Wiens et al., 2022), the vast majority of veins and other diagenetic assemblages analized by ChemCam are made of hydrated sulphate (Ca or Mg), halite (NaCl) or sylvite (KCl) (Nachon et al., 2014; L'Haridon et al., 2018). Our analysis confirms that none of the numerous diagenetic mineralization are made of pure carbonates. Jezero and Gale craters have roughly similar ages (Hesperian; Grotzinger et al., 2015; Mandon et al., 2020), and the deposits investigated within the craters by the rover are of roughly similar epoch, from the early to late Hesperian. Therefore, the absence/presence of carbonates cannot be attributed to a global evolution of the atmospheric composition over geological times. Experimental simulation of weathering of crustal rocks under a CO_2-bearing atmosphere, does not produce significant carbonate (Baron et al., 2019). A possibility is that the presence of carbonate in Jezero crater may be related to a different protolith, locally much more mafic that in Gale crater, leading to a different chemistry of the fluid and
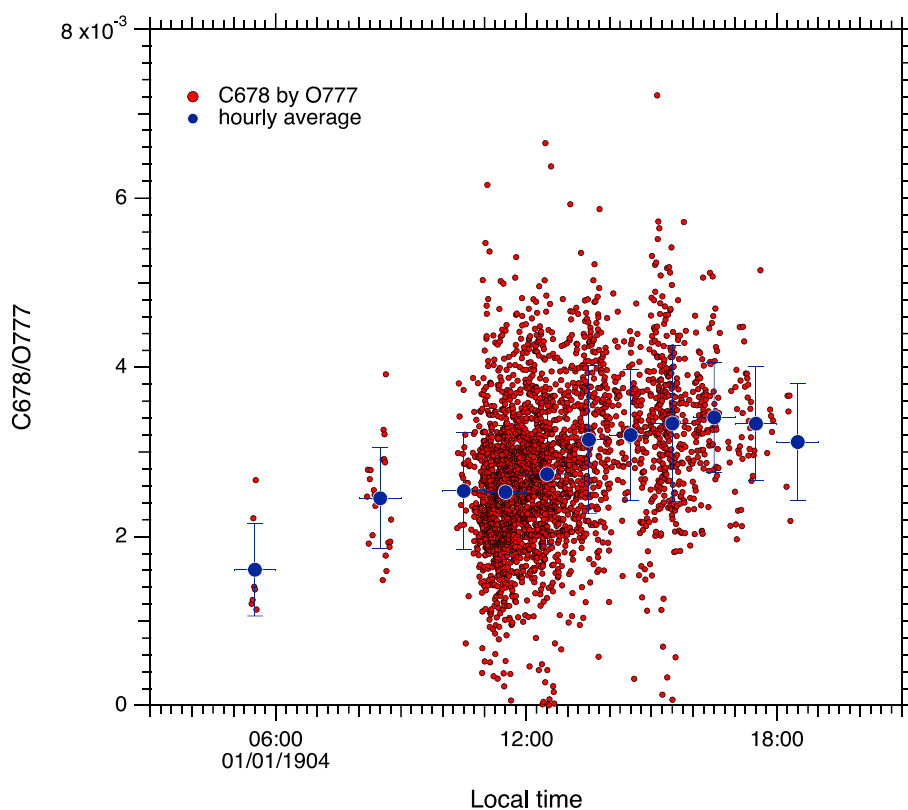

Fig. 13. Variability of the C/O ratio with local time. Only targets in the range 2.8–3.3 m were selected. The red points are individual measurements while the blue dots correspond to hourly averages. (For interpretation of the references to color in this figure legend, the reader is referred to the web version of this article.)

its precipitates. As noted by Ruff et al. (2022), the presence of carbonates on Mars seems to be associated to an elevated abundance of olivine whether in the Comanche outcrop in Gusev crater, or in the Nili Fosae area. On Earth, one of the major occurrences of Mg-rich carbonates is the hydrothermal alteration or chemical weathering of ultramafic rocks (Scheller et al., 2021). Chemical weathering of ultramafic rock will lead to Si- and Ca-poor, Fe- and Mg-rich fluids, that, pending a sufficient CO_2 activity, may promote Fe—Mg carbonate precipitation (Scheller et al., 2021). This process was initially proposed by Ehlmann et al. (2008) as the mechanism that led to the precipitation of the Nili Fossae carbonate. Altogether, the paucity of Fe—Mg carbonate in Gale may be related to the paucity of olivine in the protolith encountered so far.

5. Conclusion

We reported on laboratory studies of carbon detection with LIBS and an investigation of carbon signatures in data from the ChemCam instrument in Gale crater, Mars. We conclude that:

The detection limit of carbon with LIBS under a CO_2 atmosphere is strongly impacted by the excitation of atmospheric carbon and oxygen. This is shown by the presence of a strong correlation between carbon and oxygen emission lines. This leads to a degraded detection limit compared to analysis performed in terrestrial atmosphere. Carbon in the target can still be identified, if present in significant amount, by looking at a deviation from this correlation. Based on an analysis of carbon-rich phases (coal, carbonate) with basaltic material, the inferred single-point limit of detection is 4.5 and 6.9 wt% C for reduced and oxidized carbon respectively. This implies that, based on carbon-lines, carbonate can only be detected at high mass fractions (typically >25 wt%). These limits of detection may be lowered by combining the measurement of carbon with signatures of other carbonate-forming elements.

The C vs O correlation observed in the laboratory dataset is also found in Martian data, showing that the C signature is also dominated by an atmospheric contribution. The correlation depends on the distance to the target, probably in relation the variation of the irradiance with distance.

Based on a combined analysis of carbon lines and major element compositions (Fe,Mg,Ca), there was no detection of carbonate in the ChemCam dataset up to sol 3355 found. We estimate that carbonate therefore was not present as a major constituent (>50%) of any of the analyzed ChemCam LIBS analysis.

Declaration of Competing Interest

The authors declare that they have no known competing financial interests or personal relationships that could have appeared to influence the work reported in this paper.

Data availability

Data will be made available on request.

Acknowledgments

References

Achilles, C.N., Downs, R.T., Ming, D.W., Rampe, E.B., Morris, R.V., Treiman, A.H., Morrison, S.M., Blake, D.F., Vaniman, D.T., Ewing, R.C., Chipera, S.J., Yen, A.S., Bristow, T.F., Ehlmann, B.L., Gellert, R., Hazen, R.M., Fendrich, K.V., Craig, P.I., Grotzinger, J.P., Des Marais, D.J., Farmer, J.D., Sarrazin, P.C., Morookian, J.M., 2017. Mineralogy of an active eolian sediment from the Namib dune, Gale crater, Mars. J. Geophys. Res. (Planets) 122, 2344–2361.

Alexander, C.M.O., Bowden, R., Fogel, M.L., Howard, K.T., Herd, C.D.K., Nittler, L.R., 2012. The provenances of asteroids, and their contributions to the volatile inventories of the terrestrial planets. Science 337, 721–723. https://doi.org/10.1126/science.1223474.

Allen, C.C., Morris, R.V., Jager, K.M., Golden, D.C., Lindstrom, D.J., Lindstrom, M.M., Lockwood, J.P., 1998. Martian regolith simulant JSC Mars-1. In: Lunar and Planetary Science Conference, p. 1690.

Anderson, R.B., Clegg, S.M., Frydenvang, J., Wiens, R.C., McLennan, S., Morris, R.V., Ehlmann, B., Dyar, M.D., 2017a. Improved accuracy in quantitative laser-induced breakdown spectroscopy using sub-models. Spectrochimica Acta - Part B Atomic Spectrosc. 129, 49–57. https://doi.org/10.1016/j.sab.2016.12.002.

Anderson, D.E., Ehlmann, B.L., Forni, O., Clegg, S.M., Cousin, A., Thomas, N.H., Lasue, J., Delapp, D.M., McInroy, R.E., Gasnault, O., Dyar, M.D., Schröder, S., Maurice, S., Wiens, R.C., 2017b. Characterization of LIBS emission lines for the identification of chlorides, carbonates, and sulfates in salt/basalt mixtures for the application to MSL ChemCam data. J. Geophys. Res. (Planets). 122, 744–770.

Baron, F., Gaudin, A., Lorand, J.-P., Mangold, N., 2019. New Constraints on Early Mars Weathering Conditions From an Experimental Approach on Crust Simulants. Journal of Geophysical Research: Planets 124, 2169–9097.

Beck, P., Quirico, E., Sevestre, D., Montes-Hernandez, G., Pommerol, A., Schmitt, B., 2011. Goethite as an alternative origin of the 3.1 μm band on dark asteroids. Astron. Astrophys. 526 https://doi.org/10.1051/0004-6361/201015851.

Behar, F., Beaumont, V., Penteado, De B., 2001. Rock-eval 6 technology: performances and developments. Oil Gas Sci. Technol. 56, 111–134. https://doi.org/10.2516/ogst:2001013.

Blake, D.F., Morris, R.V., Kocurek, G., Morrison, S.M., Downs, R.T., Bish, D., Ming, D.W., Edgett, K.S., Rubin, D., Goetz, W., Madsen, M.B., Sullivan, R., Gellert, R., Campbell, I., Treiman, A.H., McLennan, S.M., Yen, A.S., Grotzinger, J., Vaniman, D.T., Chipera, S.J., Achilles, C.N., Rampe, E.B., Sumner, D., Meslin, P.-Y., Maurice, S., Forni, O., Gasnault, O., Fisk, M., Schmidt, M., Mahaffy, P., Leshin, L.A., Glavin, D., Steele, A., Freissinet, C., Navarro-González, R., Yingst, R.A., Kah, L.C., Bridges, N., Lewis, K.W., Bristow, T.F., Farmer, J.D., Crisp, J.A., Stolper, E.M., Des Marais, D.J., Sarrazin, P., Agard, C., Alves Verdasca, J.A., Anderson, Robert, Anderson, Ryan, Archer, D., Armiens-Aparicio, C., Arvidson, R., Atlaskin, E., Atreya, S., Aubrey, A., Baker, B., Baker, M., Balic-Zunic, T., Baratoux, D., Baroukh, J., Barraclough, B., Bean, K., Beegle, L., Behar, A., Bell, J., Bender, S., Benna, M., Bentz, J., Berger, G., Berger, J., Berman, D., Blanco Avalos, J.J., Blaney, D., Blank, J., Blau, H., Bleacher, L., Boehm, E., Botta, O., Böttcher, S., Boucher, T., Bower, H., Boyd, N., Boynton, B., Breves, E., Bridges, J., Brinckerhoff, W., Brinza, D., Brunet, C., Brunner, A., Brunner, W., Buch, A., Bullock, M., Burmeister, S., Cabane, M., Calef, F., Cameron, J., Cantor, B., Caplinger, M., Rodríguez, J.C., Carmosino, M., Blázquez, I.C., Charpentier, A., Choi, D., Clark, B., Clegg, S., Cleghorn, T., Cloutis, E., Cody, G., Coll, P., Conrad, P., Coscia, D., Cousin, A., Cremers, D., Cros, A., Cucinotta, F., d'Uston, C., Davis, S., Day, M., Juarez, M. De La T., DeFlores, L., DeLapp, D., DeMarines, J., Dietrich, W., Dingler, R., Donny, C., Drake, D., Dromart, G., Dupont, A., Duston, B., Dworkin, J., Dyar, M. D., Edgar, L., Edwards, C., Edwards, L., Ehlmann, B., Ehresmann, B., Eigenbrode, J., Elliott, B., Elliott, H., Ewing, R., Fabre, C., Fairén, A., Farley, K., Fassett, C., Favot, L., Fay, D., Fedosov, F., Feldman, J., Feldman, S., Fitzgibbon, M., Flesch, G., Floyd, M., Flückiger, L., Fraeman, A., Francis, R., François, P., Franz, H., French, K.L., Frydenvang, J., Gaboriaud, A., Gailhanou, M., Garvin, J., Geffroy, C., Genzer, M., Godber, A., Goesmann, F., Golovin, D., Gómez, F.G., Gómez-Elvira, J., Gondet, B., Gordon, S., Gorevan, S., Grant, J., Griffes, J., Grinspoon, D., Guillemot, P., Guo, J., Gupta, S., Guzewich, S., Haberle, R., Halleaux, D., Hallet, B., Hamilton, V., Hardgrove, C., Harker, D., Harpold, D., Harri, A.-M., Harshman, K., Hassler, D., Haukka, H., Hayes, A., Herkenhoff, K., Herrera, P., Hettrich, S., Heydari, E., Hipkin, V., Hoehler, T., Hollingsworth, J., Hudgins, J., Huntress, W., Hurowitz, J., Hviid, S., Iagnemma, K., Indyk, S., Israël, G., Jackson, R., Jacob, S., Jakosky, B., Jensen, E., Jensen, J.K., Johnson, J., Johnson, M., Johnstone, S., Jones, A., Jones, J., Joseph, J., Jun, I., Kahanpää, H., Kahre, M., Karpushkina, N., Kasprzak, W., Kauhanen, J., Keely, L., Kemppinen, O., Keymeulen, D., Kim, M.-H., Kinch, K., King, P., Kirkland, L., Koefoed, A., Köhler, J., Kortmann, O., Kozyrev, A., Krezoski, J., Krysak, D., Kuzmin, R., Lacour, J.L., Lafaille, V., Langevin, Y., Lanza, N., Lasue, J., Le Mouélic, S., Lee, E.M., Lee, Q.-M., Lees, D., Lefavor, M., Lemmon, M., Lepinette Malvitte, A., Léveillé, R., Lewin-Carpintier, É., Li, S., Lipkaman, L., Little, C., Litvak, M., Lorigny, E., Lugmair, G., Lundberg, A., Lyness, E., Maki, J., Malakhov, A., Malespin, C., Malin, M., Mangold, N., Manning, H., Marchand, G., Marín Jiménez, M., Martín García, C., Martin, D., Martin, M., Martínez-Frías, J., Martín-Soler, J., Martín-Torres, F.J., Mauchien, P., McAdam, A., McCartney, E., McConnochie, T., McCullough, E., McEwan, I., McKay, C., McNair, S., Melikechi, N., Meyer, M., Mezzacappa, A., Miller, H., Miller, K., Milliken, R., Minitti, M., Mischna, M., Mitrofanov, I., Moersch, J., Mokrousov, M., Molina Jurado, A., Moores, J., Mora-Sotomayor, L., Morookian, J. M., Mueller-Mellin, R., Muller, J.-P., Muñoz Caro, G., Nachon, M., Navarro López, S., Nealson, K., Nefian, A., Nelson, T., Newcombe, M., Newman, C., Newsom, H., Nikiforov, S., Niles, P., Nixon, B., Dobrea, E.N., Nolan, T., Oehler, D., Ollila, A., Olson, T., Owen, T., Pablo, H., Paillet, A., Pallier, E., Palucis, M., Parker, T., Parot, Y., Patel, K., Paton, M., Paulsen, G., Pavlov, A., Pavri, B., Peinado-González, V., Pepin, R., Peret, L., Perez, R., Perrett, G., Peterson, J., Pilorget, C., Pinet, P., Pla-García, J., Plante, I., Poitrasson, F., Polkko, J., Popa, R., Posiolova, L., Pradler, I., Prats, B., Prokhorov, V., Purdy, S.W., Raaen, E., Radziemski, L., Rafkin, S., Ramos, M., Raulin, F., Ravine, M., Reitz, G., Rennó, N., Rice, M., Richardson, M., Robert, F., Rodriguez Manfredi, J.A., Romeral-Planelló, J.J., Rowland, S., Saccoccio, M., Salamon, A., Sandoval, J., Sanin, A., Sans Fuentes, S.A., Saper, L., Sautter, V., Savijärvi, H., Schieber, J., Schmidt, W., Scholes, D., Schoppers, M., Schröder, S., Sebastian Martinez, E., Sengstacken, A., Shterts, R., Siebach, K., Siili, T., Simmonds, J., Sirven, J.-B., Slavney, S., Sletten, R., Smith, M., Sobrón Sánchez, P., Spanovich, N., Spray, J., Squyres, S., Stack, K., Stalport, F., Stein, T., Stern, J., Stewart, N., Stipp, S.L.S.,

P. Beck et al.

Icarus 408 (2024) 115840

Stoiber, K., Sucharski, B., Summons, R., Sun, V., Supulver, K., Sutter, B., Szopa, C., Tate, C., Teinturier, S., ten Kate, I.L., Thomas, P., Thompson, L., Tokar, R., Toplis, M., Torres Redondo, J., Trainer, M., Tretyakov, V., Urqui-O'Callaghan, R., Van Beek, J., Van Beek, T., VanBommel, S., Varenikov, A., Vasavada, A., Vasconcelos, P., Vicenzi, E., Vostrukhin, A., Voytek, M., Wadhwa, M., Ward, J., Webster, C., Weigle, E., Wellington, D., Westall, F., Wiens, R.C., Wilhelm, M.B., Williams, A., Williams, J., Williams, R., Williams, R.B., Wilson, N., Wimmer-Schweingruber, R., Wolff, M., Wong, M., Wray, J., Wu, M., Yana, C., Zeitlin, C., Zimdar, R., Zorzano Mier, M.-P., Team, M.S.L., 2013. Curiosity at gale crater, mars: characterization and analysis of the rocknest sand shadow. Science 341, 1239505.

Bultel, B., Quantin-Nataf, C., Andréani, M., Clénet, H., Lozac'h, L., 2015. Deep alteration between Hellas and Isidis basins. Icarus 260, 141–160.

Chen, J., Pisonero, J., Chen, S., Wang, X., Fan, Q., Duan, Y., 2020. Convolutional neural network as a novel classification approach for laser-induced breakdown spectroscopy applications in lithological recognition. Spectrochim. Acta B At. Spectrosc. 166, 105801 https://doi.org/10.1016/j.sab.2020.105801.

Clavé, E., Benzerara, K., Meslin, P.-Y., Forni, O., Royer, C., Mandon, L., Beck, P., Quantin-Nataf, C., Beyssac, O., Cousin, A., Bousquet, B., Wiens, R.C., Maurice, S., Dehouck, E., Schröder, S., Gasnault, O., Mangold, N., Dromart, G., Bosak, T., Bernard, S., Udry, A., Anderson, R.B., Arana, C., Brown, A.J., Castro, K., Clegg, S.M., Cloutis, E., Fairén, A.G., Flannery, D.T., Gasda, P.J., Johnson, J.R., Lasue, J., Lopez-Reyes, G., Madariaga, J.M., Manrique, J.A., Le Mouélic, S., Núñez, J.I., Ollila, A.M., Pilleri, P., Pilorget, C., Pinet, P., Poulet, F., Veneranda, M., Wolf, Z.U., the SuperCam team, 2023. Carbonate detection with supercam in igneous rocks on the floor of Jezero Crater, Mars. J. Geophys. Res. Planets 128. https://doi.org/10.1029/2022JE007463 e2022JE007463.

Clegg, S.M., Wiens, R.C., Anderson, R., Forni, O., Frydenvang, J., Lasue, J., Cousin, A., Payré, V., Boucher, T., Dyar, M.D., McLennan, S.M., Morris, R.V., Graff, T.G., Mertzman, S.A., Ehlmann, B.L., Belgacem, I., Newsom, H., Clark, B.C., Melikechi, N., Mezzacappa, A., McInroy, R.E., Martinez, R., Gasda, P., Gasnault, O., Maurice, S., 2017. Recalibration of the Mars science laboratory ChemCam instrument with an expanded geochemical database. Spectrochimica Acta - Part B Atomic Spectrosc. 129, 64–85. https://doi.org/10.1016/j.sab.2016.12.003.

Cousin, A., Meslin, P.Y., Wiens, R.C., Rapin, W., Mangold, N., Fabre, C., Gasnault, O., Forni, O., Tokar, R., Ollila, A., Schröder, S., Lasue, J., Maurice, S., Sautter, V., Newsom, H., Vaniman, D., Le Mouélic, S., Dyar, D., Berger, G., Blaney, D., Nachon, M., Dromart, G., Lanza, N., Clark, B., Clegg, S., Goetz, W., Berger, J., Barraclough, B., Delapp, D., 2015. Compositions of coarse and fine particles in martian soils at gale: a window into the production of soils. Icarus 249, 22–42.

Cousin, A., Sautter, V., Fabre, C., Dromart, G., Montagnac, G., Drouet, C., Meslin, P.Y., Gasnault, O., Beyssac, O., Bernard, S., Cloutis, E., Forni, O., Beck, P., Fouchet, T., Johnson, J.R., Lasue, J., Ollila, A.M., De Parseval, P., Gouy, S., Caron, B., Madariaga, J.M., Arana, G., Madsen, M.B., Laserna, J., Moros, J., Manrique, J.A., Lopez-Reyes, G., Rull, F., Maurice, S., Wiens, R.C., 2022. SuperCam calibration targets on board the perseverance rover: Fabrication and quantitative characterization. Spectrochim 188, 106341.

Currie, L.A., 1968. Limits for qualitative detection and quantitative determination. Application to radiochemistry. Anal. Chem. 40, 586–593. https://doi.org/10.1021/ac60259a007.

Dehouck, E., Cousin, A., Mangold, N., Frydenvang, J., Gasnault, O., Forni, O., Rapin, W., Gasda, P.J., Caravaca, G., David, G., Bedford, C.C., Lasue, J., Meslin, P.-Y., Rammelkamp, K., Desjardins, M., Le Mouélic, S., Thorpe, M.T., Fox, V.K., Bennett, K. A., Bryk, A.B., Lanza, N.L., Maurice, S., Wiens, R.C., 2022. Bedrock geochemistry and alteration history of the clay-bearing Glen Torridon Region of Gale Crater, Mars. J. Geophys. Res. Planets 127. https://doi.org/10.1029/2021JE007103.

Dequaire, T., Meslin, P.-Y., Beck, P., Jaber, M., Cousin, A., Rapin, W., Lasne, J., Gasnault, O., Maurice, S., Buch, A., Szopa, C., Coll, P., 2017. Analysis of carbon and nitrogen signatures with laser-induced breakdown spectroscopy; the quest for organics under Mars-like conditions. Spectrochimica Acta - Part B Atomic Spectrosc. 131, 8–17. https://doi.org/10.1016/j.sab.2017.02.015.

Ehlmann, B.L., Buz, J., 2015. Mineralogy and fluvial history of the watersheds of Gale, Knobel, and sharp craters: A regional context for the Mars science laboratory Curiosity's exploration. Geophys. Res. Lett. 42, 264–273. https://doi.org/10.1002/2014GL062553.

Ehlmann, B.L., Mustard, J.F., Murchie, S.L., Poulet, F., Bishop, J.L., Brown, A.J., Calvin, W.M., Clark, R.N., Des Marais, D.J., Milliken, R.E., Roach, L.H., Roush, T.L., Swayze, G.A., Wray, J.J., 2008. Orbital identification of carbonate-bearing rocks on mars. Science 322, 1828.

Ehlmann, B.L., Mustard, J.F., Murchie, S.L., Bibring, J.-P., Meunier, A., Fraeman, A.A., Langevin, Y., 2011. Subsurface water and clay mineral formation during the early history of Mars. Nature 479, 53–60.

Eigenbrode, J.L., Summons, R.E., Steele, A., Freissinet, C., Millan, M., Navarro-González, R., Sutter, B., McAdam, A.C., Franz, H.B., Glavin, D.P., Archer, P.D., Mahaffy, P.R., Conrad, P.G., Hurowitz, J.A., Grotzinger, J.P., Gupta, S., Ming, D.W., Sumner, D.Y., Szopa, C., Malespin, C., Buch, A., Coll, P., 2018. Organic matter preserved in 3-billion-year-old mudstones at Gale crater. Mars 360, 1096–1101.

Fabre, C., Maurice, S., Cousin, A., Wiens, R.C., Forni, O., Sautter, V., Guillaume, D., 2011. Onboard calibration igneous targets for the mars science laboratory curiosity rover and the chemistry camera laser induced breakdown spectroscopy instrument. Spectrochimica Acta - Part B Atomic Spectrosc. 66, 280–289. https://doi.org/10.1016/j.sab.2011.03.012.

Farley, K.A., Stack, K.M., Shuster, D.L., Horgan, B.H.N., Hurowitz, J.A., Tarnas, J.D., Simon, J.I., Sun, V.Z., Scheller, E.L., Moore, K.R., McLennan, S.M., Vasconcelos, P. M., Wiens, R.C., Treiman, A.H., Mayhew, L.E., Beyssac, O., Kizovski, T.V., Tosca, N. J., Williford, K.H., Crumpler, L.S., Beegle, L.W., Bell, J.F., Ehlmann, B.L., Liu, Y., Maki, J.N., Schmidt, M.E., Allwood, A.C., Amundsen, H.E.F., Bhartia, R., Bosak, T.,

Brown, A.J., Clark, B.C., Cousin, A., Forni, O., Gabriel, T.S.J., Goreva, Y., Gupta, S., Hamran, S.-E., Herd, C.D.K., Hickman-Lewis, K., Johnson, J.R., Kah, L.C., Kelemen, P.B., Kinch, K.B., Mandon, L., Mangold, N., Quantin-Nataf, C., Rice, M.S., Russell, P. S., Sharma, S., Siljeström, S., Steele, A., Sullivan, R., Wadhwa, M., Weiss, B.P., Williams, A.J., Wogsland, B.V., Willis, P.A., Acosta-Maeda, T.A., Beck, P., Benzerara, K., Bernard, S., Burton, A.S., Cardarelli, E.L., Chide, B., Clavé, E., Cloutis, E.A., Cohen, B.A., Czaja, A.D., Debaille, V., Dehouck, E., Fairén, A.G., Flannery, D.T., Fleron, S.Z., Fouchet, T., Frydenvang, J., Garczynski, B.J., Gibbons, E.F., Hausrath, E.M., Hayes, A.G., Henneke, J., Jørgensen, J.L., Kelly, E.M., Lasue, J., Le Mouélic, S., Madariaga, J.M., Maurice, S., Merusi, M., Meslin, P.-Y., Milkovich, S.M., Million, C. C., Moeller, R.C., Núñez, J.I., Ollila, A.M., Paar, G., Paige, D.A., Pedersen, D.A.K., Pilleri, P., Pilorget, C., Pinet, P.C., Rice, J.W., Royer, C., Sautter, V., Schulte, M., Sephton, M.A., Sharma, S.K., Sholes, S.F., Spanovich, N., St. Clair, M., Tate, C.D., Uckert, K., VanBommel, S.J., Yanchilina, A.G., Zorzano, M.P., 2022. Aqueously altered igneous rocks sampled on the floor of Jezero crater, Mars. Science 377, 2196.

Flynn, G.J., 1996. The delivery of organic matter from asteroids and comets to the early surface of Mars. Earth Moon Planet. 72, 469–474. https://doi.org/10.1007/BF00117551.

Foley, C.N., Economou, T., Clayton, R.N., 2003. Final chemical results from the Mars pathfinder alpha proton X-ray spectrometer. J. Geophys. Res. (Planets) 108, 8096.

Forget, F., Hourdin, F., Fournier, R., Hourdin, C., Talagrand, O., Collins, M., Lewis, S.R., Read, P.L., Huot, J.-P., 1999. Improved general circulation models of the Martian atmosphere from the surface to above 80 km. J. Geophys. 104, 24155–24176.

Formisano, V., Atreya, S., Encrenaz, T., Ignatiev, N., Giuranna, M., 2004. Detection of methane in the atmosphere of mars. Science 306, 1758–1761.

Freissinet, C., Glavin, D.P., Mahaffy, P.R., Miller, K.E., Eigenbrode, J.L., Summons, R.E., Brunner, A.E., Buch, A., Szopa, C., Archer, P.D., Franz, H.B., Atreya, S.K., Brinckerhoff, W.B., Cabane, M., Coll, P., Conrad, P.G., Des Marais, D.J., Dworkin, J. P., Fairén, A.G., François, P., Grotzinger, J.P., Kashyap, S., ten Kate, I.L., Leshin, L.A., Malespin, C.A., Martin, M.G., Martin-Torres, J.F., McAdam, A.C., Ming, D.W., Navarro-González, R., Pavlov, A.A., Prats, B.D., Squyres, S.W., Steele, A., Stern, J.C., Sumner, D.Y., Sutter, B., Zorzano, M.-P., Team, M.S.L., 2015. Organic molecules in the Sheepbed Mudstone, Gale Crater, Mars. J. Geophys. Res. (Planets) 120, 495–514.

Gasnault, O., et al.. ChemCam Remote Micro Imager Performance. https://ui.adsabs.harvard.edu/abs/2017LPI....48.2995G.

Gasnault, O., Forni, O., Mangold, N., Wiens, R., Meslin, P.-Y., Lasue, J., Pinet, P., Maurice, S., Lewin, E., Anderson, R., Clark, B., Melikechi, N., Newsom, H., Sautter, V., Blank, J., 2015a. Updated perspective on ChemCam data through clustering. In: 46th Annual Lunar and Planetary Science Conference, p. 2789.

Gasnault, O., Forni, O., Mangold, N., Wiens, R., Meslin, P.-Y., Lasue, J., Pinet, P., Maurice, S., Lewin, E., Anderson, R., Clark, B., Melikechi, N., Newsom, H., Sautter, V., Blank, J., 2015b. Updated perspective on ChemCam data through clustering. In: 46th Annual Lunar and Planetary Science Conference, p. 2789.

Giuranna, M., Viscardy, S., Daerden, F., Neary, L., Etiope, G., Oehler, D., Formisano, V., Aronica, A., Wolkenberg, P., Aoki, S., Cardesín-Moinelo, A., Marín-Yaseli de la Parra, J., Merritt, D., Amoroso, M., 2019. Independent confirmation of a methane spike on Mars and a source region east of Gale crater. Nat 12, 326–332.

Goetz, W., Brinckerhoff, W.B., Arevalo, R., Freissinet, C., Getty, S., Glavin, D.P., Siljeström, S., Buch, A., Stalport, F., Grubisic, A., Li, X., Pinnick, V., Danell, R., van Amerom, F.H.W., Goesmann, F., Steininger, H., Grand, N., Raulin, F., Szopa, C., Meierhenrich, U., Brucato, J.R., 2016. MOMA: the challenge to search for organics and biosignatures on Mars. Int. J. 15, 239–250.

Horgan, B.H.N., Anderson, R.B., Dromart, G., Amador, E.S., Rice, M.S., 2020. The mineral diversity of Jezero crater: evidence for possible lacustrine carbonates on Mars. Icarus 339, 113526.

King, R.B., 1948. Relative transition probabilities of the swan bands of carbon. Astrophys. J. 108, 429.

Korablev, O., Avandaele, A.C., Montmessin, F., Fedorova, A.A., Trokhimovskiy, A., Forget, F., Lefèvre, F., Daerden, F., Thomas, I.R., Trompet, L., Erwin, J.T., Aoki, S., Robert, S., Neary, L., Viscardy, S., Grigoriev, A.V., Ignatiev, N.I., Shakun, A., Patrakeev, A., Belyaev, D.A., Bertaux, J.L., Olsen, K.S., Baggio, L., Alday, J., Ivanov, Y.S., Ristic, B., Mason, J., Willame, Y., Depiesse, C., Hetey, L., Berkenbosch, S., Clairquin, R., Queirolo, C., Beeckman, B., Neefs, E., Patel, M.R., Bellucci, G., López-Moreno, J.-J., Wilson, C.F., Etiope, G., Zelenyi, L., Svedhem, H., Vago, J.L., Team, A., Team, N.S., Alonso-Rodrigo, G., Altieri, F., Anufreychik, K., Arnold, G., Bauduin, S., Bolsée, D., Carrozzo, G., Clancy, R.T., Cloutis, E., Crismani, M., da Pieve, F., D'Aversa, E., Duxbury, N., Encrenaz, T., Fouchet, T., Funke, B., Fussen, D., Garcia-Comas, M., Gérard, J.-C., Giuranna, M., Gkouvelis, L., Gonzalez-Galindo, F., Grassi, D., Guerlet, S., Hartogh, P., Holmes, J., Hubert, B., Kaminski, J., Karatekin, O., Kasaba, Y., Kass, D., Khatuntsev, I., Kleinböhl, A., Kokonkov, N., Krasnopolsky, V., Kuzmin, R., Lacombe, G., Lanciano, O., Lellouch, E., Lewis, S., Luginin, M., Liuzzi, G., López-Puertas, M., López-Valverde, M., Määttänen, A., Mahieux, A., Marcq, E., Martin-Torres, J., Maslov, I., Medvedev, A., Millour, E., Moshkin, B., Mumma, M.J., Nakagawa, H., Novak, R.E., Oliva, F., Patsaev, D., Piccialli, A., Quantin-Nataf, C., Renotte, E., Ritter, B., Rodin, A., Schmidt, F., Schneider, N., Shematovich, V., Smith, M.D., Teanby, N.A., Thiemann, E., Thomas, N., Vander Auwera, J., Vazquez, L., Villanueva, G., Vincendon, M., Whiteway, J., Wilquet, V., Wolff, M.J., Wolkenberg, P., Yelle, R., Young, R., Zasova, L., Zorzano, M.P., 2019. No detection of methane on Mars from early ExoMars trace gas orbiter observations. Nature.568 517–520.

Lasue, J., Meslin, P.Y., Sautter, V., Maroger, I., Krämer Ruggiu, L., Bridges, J.C., Lewin, E., Wiens, R.C., Beck, P., Cousin, A., Forni, O., Gasnault, O., Goetz, W., Johnson, J.R., Le Mouélic, S., Nachon, M., Newsom, H., Maurice, S., Wellington, D. F., 2019. Probable chondritic fragments detected by ChemCam in Gale crater. In: 50th Annual Lunar and Planetary Science Conference, p. 2274.

16

Lasue, J., Meslin, P.-Y., Cohen, B.A., Sautter, V., Bridges, J.C., Lewin, E., Wiens, R.C., Beck, P., Cousin, A., Forni, O., Gasnault, O., Goetz, W., Johnson, J.R., Le Mouélic, S., Nachon, M., Newsom, H., Maurice, S., 2020. Gretna Green, a possible chondrite detected at Glen Torridon in Gale Crater. In: 51st annual lunar and planetary science conference, p. 2125.

Leshin, L.A., Mahaffy, P.R., Webster, C.R., Cabane, M., Coll, P., Conrad, P.G., Archer, P. D., Atreya, S.K., Brunner, A.E., Buch, A., Eigenbrode, J.L., Flesch, G.J., Franz, H.B., Freissinet, C., Glavin, D.P., McAdam, A.C., Miller, K.E., Ming, D.W., Morris, R.V., Navarro-González, R., Niles, P.B., Owen, T., Pepin, R.O., Squyres, S., Steele, A., Stern, J.C., Summons, R.E., Sumner, D.Y., Sutter, B., Szopa, C., Teinturier, S., Trainer, M.G., Wray, J.J., Grotzinger, J.P., Kemppinen, O., Bridges, N., Johnson, J. R., Minitti, M., Cremers, D., Bell, J.F., Edgar, L., Farmer, J., Godber, A., Wadhwa, M., Wellington, D., McEwan, I., Newman, C., Richardson, M., Charpentier, A., Peret, L., King, P., Blank, J., Weigle, G., Schmidt, M., Li, S., Milliken, R., Robertson, K., Sun, V., Baker, M., Edwards, C., Ehlmann, B., Farley, K., Griffes, J., Miller, H., Newcombe, M., Pilorget, C., Rice, M., Siebach, K., Stack, K., Stolper, E., Brunet, C., Hipkin, V., Léveillé, R., Marchand, G., Sánchez, P.S., Favot, L., Cody, G., Flückiger, L., Lees, D., Nefian, A., Martin, M., Gailhanou, M., Westall, F., Israël, G., Agard, C., Baroukh, J., Donny, C., Gaboriaud, A., Guillemot, P., Lafaille, V., Lorigny, E., Paillet, A., Pérez, R.S., Yana, C., Armiens-Aparicio, C., Rodríguez, J.C., Blázquez, I.C., Gómez, F.G., Gómez-Elvira, J., Hettrich, S., Malvitte, A.L., Jiménez, M.M., Martínez-Frías, J., Martín-Soler, J., Martín-Torres, F.J., Jurado, A. M., Mora-Sotomayor, L., Caro, G.M., López, S.N., Peinado-González, V., Pla-García, J., Manfredi, J.A.R., Romeral-Planelló, J.J.F., Martinez, E.S., Redondo, J.T., Urqui-O'Callaghan, R., Mier, M.-P.Z., Chipera, S., Lacour, J.-L., Mauchien, P., Sirven, J.-B., Manning, H., Fairén, A., Hayes, A., Joseph, J., Sullivan, R., Thomas, P., Dupont, A., Lundberg, A., Melikechi, N., Mezzacappa, A., DeMarines, J., Grinspoon, D., Reitz, G., Prats, B., Atlaskin, E., Genzer, M., Harri, A.-M., Haukka, H., Kahanpää, H., Kauhanen, J., Kemppinen, O., Paton, M., Polkko, J., Schmidt, W., Siili, T., Fabre, C., Wilhelm, M.B., Poitrasson, F., Patel, K., Gorevan, S., Indyk, S., Paulsen, G., Gupta, S., Bish, D., Schieber, J., Gondet, B., Langevin, Y., Geffroy, C., Baratoux, D., Berger, G., Cros, A., d'Uston, C., Forni, O., Gasnault, O., Lasue, J., Lee, Q.-M., Maurice, S., Meslin, P.-Y., Pallier, E., Parot, Y., Pinet, P., Schröder, S., Toplis, M., Lewin, É., Brunner, W., Heydari, E., Achilles, C., Oehler, D., Coscia, D., Israël, G., Dromart, G., Robert, F., Sautter, V., Le Mouélic, S., Mangold, N., Nachon, M., Stalport, F., François, P., Raulin, F., Cameron, J., Clegg, S., Cousin, A., DeLapp, D., Dingler, R., Jackson, R.S., Johnstone, S., Lanza, N., Little, C., Nelson, T., Wiens, R.C., Williams, R.B., Jones, A., Kirkland, L., Treiman, A., Baker, B., Cantor, B., Caplinger, M., Davis, S., Duston, B., Edgett, K., Fay, D., Hardgrove, C., Harker, D., Herrera, P., Jensen, E., Kennedy, M.R., Krezoski, G., Krysak, D., Lipkaman, L., Malin, M., McCartney, E., McNair, S., Nixon, B., Posiolova, L., Ravine, M., Salamon, A., Saper, L., Stoiber, K., Supulver, K., Van Beek, J., Van Beek, T., Zimdar, R., French, K.L., Iagnemma, K., Goesmann, F., Goetz, W., Hviid, S., Johnson, M., Lefavor, M., Lyness, E., Breves, E., Dyar, M.D., Fassett, C., Blake, D.F., Bristow, T., DesMarais, D., Edwards, L., Haberle, R., Hoehler, T., Hollingsworth, J., Kahre, M., Keely, L., McKay, C., Wilhelm, M.B., Bleacher, L., Brinckerhoff, W., Choi, D., Dworkin, J.P., Floyd, M., Garvin, J., Harpold, D., Jones, A., Martin, D.K., Pavlov, A., Raaen, E., Smith, M.D., Tan, F., Meyer, M., Posner, A., Voytek, M., Anderson, R.C., Aubrey, A., Beegle, L.W., Behar, A., Blaney, D., Brinza, D., Calef, F., Christensen, L., Crisp, J.A., DeFlores, L., Ehlmann, B., Feldman, J., Feldman, S., Hurowitz, J., Jun, I., Keymeulen, D., Maki, J., Mischna, M., Morookian, J.M., Parker, T., Pavri, B., Schoppers, M., Sengstacken, A., Simmonds, J.J., Spanovich, N., Juarez, M. De La T., Vasavada, A.R., Yen, A., Cucinotta, F., Jones, J.H., Rampe, E., Nolan, T., Fisk, M., Radziemski, L., Barraclough, B., Bender, S., Berman, D., Dobrea, E.N., Tokar, R., Vaniman, D., Williams, R.M.E., Yingst, A., Lewis, K., Cleghorn, T., Huntress, W., Manhès, G., Hudgins, J., Olson, T., Stewart, N., Sarrazin, P., Grant, J., Vicenzi, E., Wilson, S.A., Bullock, M., Ehresmann, B., Hamilton, V., Hassler, D., Peterson, J., Rafkin, S., Zeitlin, C., Fedosov, F., Golovin, D., Karpushkina, N., Kozyrev, A., Litvak, M., Malakhov, A., Mitrofanov, I., Mokrousov, M., Nikiforov, S., Prokhorov, V., Sanin, A., Tretyakov, V., Varenikov, A., Vostrukhin, A., Kuzmin, R., Clark, B., Wolff, M., McLennan, S., Botta, O., Drake, D., Bean, K., Lemmon, M., Schwenzer, S.P., Anderson, R.B., Herkenhoff, K., Lee, E.M., Sucharski, R., Hernández, M.Á., de Ávalos, J.J.B., Ramos, M., Kim, M.-H., Malespin, C., Plante, I., Muller, J.-P., Ewing, R., Boynton, W., Downs, R., Fitzgibbon, M., Harshman, K., Morrison, S., Dietrich, W., Kortmann, O., Palucis, M., Williams, A., Lugmair, G., Wilson, M.A., Rubin, D., Jakosky, B., Balic-Zunic, T., Frydenvang, J., Jensen, J.K., Kinch, K., Koefoed, A., Madsen, M.B., Stipp, S.L.S., Boyd, N., Campbell, J.L., Gellert, R., Perrett, G., Pradler, I., VanBommel, S., Jacob, S., Rowland, S., Atlaskin, E., Savijärvi, H., Boehm, E., Böttcher, S., Burmeister, S., Guo, J., Köhler, J., García, C.M., Mueller-Mellin, R., Wimmer-Schweingruber, R., Bridges, J.C., McConnochie, T., Benna, M., Bower, H., Blau, H., Boucher, T., Carmosino, M., Elliott, H., Halleaux, D., Rennó, N., Wong, M., Elliott, B., Spray, J., Thompson, L., Gordon, S., Newsom, H., Ollila, A., Williams, J., Vasconcelos, P., Bentz, J., Nealson, K., Popa, R., Kah, L.C., Moersch, J., Tate, C., Day, M., Kocurek, G., Hallet, B., Sletten, R., Francis, R., McCullough, E., Cloutis, E., Ten Kate, I.L., Kuzmin, R., Arvidson, R., Fraeman, A., Scholes, D., Slavney, S., Stein, T., Ward, J., Berger, J., Moores, J.E., Team, M.S., 2013. Volatile, isotope, and organic analysis of martian fines with the mars curiosity rover. Scienc 341, 1238937.

L'Haridon, J., Mangold, N., Meslin, P.-Y., Johnson, J.R., Rapin, W., Forni, O., Cousin, A., Payré, V., Dehouck, E., Nachon, M., Le Deit, L., Gasnault, O., Maurice, S., Wiens, R. C., 2018. Chemical variability in mineralized veins observed by ChemCam on the lower slopes of Mount Sharp in Gale crater. Mars 311, 69–86.

Mangold, N., Dehouck, E., Fedo, C., Forni, O., Achilles, C., Bristow, T., Downs, R.T., Frydenvang, J., Gasnault, O., L'Haridon, J., Le Deit, L., Maurice, S., McLennan, S.M., Meslin, P.-Y., Morrison, S., Newsom, H.E., Rampe, E., Rapin, W., Rivera-Hernandez, F., Salvatore, M., Wiens, R.C., 2019. Chemical alteration of fine-grained

sedimentary rocks at Gale crater. Icarus 321, 619–631. https://doi.org/10.1016/j. icarus.2018.11.004.

Manrique, J.A., Lopez-Reyes, G., Cousin, A., Rull, F., Maurice, S., Wiens, R.C., Madsen, M.B., Madariaga, J.M., Gasnault, O., Aramendia, J., Arana, G., Beck, P., Bernard, S., Bernardi, P., Bernt, M.H., Berrocal, A., Beyssac, O., Caïs, P., Castro, C., Castro, K., Clegg, S.M., Cloutis, E., Dromart, G., Drouet, C., Dubois, B., Escribano, D., Fabre, C., Fernandez, A., Forni, O., Garcia-Baonza, V., Gontijo, I., Johnson, J., Laserna, J., Lasue, J., Madsen, M., Mateo-Marti, E., Medina, J., Meslin, P.-Y., Montagnac, G., Moral, A., Moros, J., Ollila, A.M., Ortega, C., Prieto-Ballesteros, O., Reess, J.M., Robinson, S., Rodriguez, J., Saiz, J., Sanz-Arranz, J.A., Sard, I., Sautter, V., Sobron, P., Toplis, M., Veneranda, M., 2020. SuperCam calibration targets: design and development. Space Sci. 216, 138.

Maurice, S., Clegg, S.M., Wiens, R.C., Gasnault, O., Rapin, W., Forni, O., Cousin, A., Sautter, V., Mangold, N., Le Deit, L., Nachon, M., Anderson, R.B., Lanza, N.L., Fabre, C., Payré, V., Lasue, J., Meslin, P.-Y., Léveillé, R.J., Barraclough, B.L., Beck, P., Bender, S.C., Berger, G., Bridges, J.C., Bridges, N.T., Dromart, G., Dyar, M. D., Francis, R., Frydenvang, J., Gondet, B., Ehlmann, B.L., Herkenhoff, K.E., Johnson, J.R., Langevin, Y., Madsen, M.B., Melikechi, N., Lacour, J.-L., Le Mouélic, S., Lewin, E., Newsom, H.E., Ollila, A.M., Pinet, P., Schröder, S., Sirven, J.-B., Tokar, R.L., Toplis, M.J., D'Uston, C., Vaniman, D.T., Vasavada, A.R., 2016. ChemCam activities and discoveries during the nominal mission of the Mars science laboratory in Gale crater, Mars. J. Anal. At. Spectrom. 31, 863–889. https://doi.org/ 10.1039/c5ja00417a.

Maurice, S., Wiens, R.C., Bernardi, P., Caïs, P., Robinson, S., Nelson, T., Gasnault, O., Reess, J.-M., Deleuze, M., Rull, F., Manrique, J.-A., Abbaki, S., Anderson, R.B., André, Y., Angel, S.M., Arana, G., Battault, T., Beck, P., Benzerara, K., Bernard, S., Berthias, J.-P., Beyssac, O., Bonafous, M., Bousquet, B., Boutillier, M., Cadu, A., Castro, K., Chapron, F., Chide, B., Clark, K., Clavé, E., Clegg, S., Cloutis, E., Collin, C., Cordoba, E.C., Cousin, A., Dameury, J.-C., D'Anna, W., Daydou, Y., Debus, A., Deflores, L., Dehouck, E., Delapp, D., De Los Santos, G., Donny, C., Doressoundiram, A., Dromart, G., Dubois, B., Dufour, A., Dupieux, M., Egan, M., Ervin, J., Fabre, C., Fau, A., Fischer, W., Forni, O., Fouchet, T., Frydenvang, J., Gauffre, S., Gauthier, M., Gharakanian, V., Gilard, O., Gontijo, I., Gonzalez, R., Granena, D., Grotzinger, J., Hassen-Khodja, R., Heim, M., Hello, Y., Hervet, G., Humeau, O., Jacob, X., Jacquinod, S., Johnson, J.R., Kouach, D., Lacombe, G., Lanza, N., Lapauw, L., Laserna, J., Lasue, J., Le Deit, L., Le Mouélic, S., Le Comte, E., Lee, Q.-M., Legett, C., Leveille, R., Lewin, E., Leyrat, C., Lopez-Reyes, G., Lorenz, R., Lucero, B., Madariaga, J.M., Madsen, S., Madsen, M., Mangold, N., Manni, F., Mariscal, J.-F., Martinez-Frias, J., Mathieu, K., Mathon, R., McCabe, K.P., McConnochie, T., McLennan, S.M., Mekki, J., Melikechi, N., Meslin, P.-Y., Micheau, V., Michel, Y., Michel, J.M., Mimoun, D., Misra, A., Montagnac, G., Montaron, C., Montmessin, F., Moros, J., Mousset, V., Morizet, Y., Murdoch, N., Newell, R.T., Newsom, H., Nguyen Tuong, N., Ollila, A.M., Orttner, G., Oudda, L., Pares, L., Parisot, J., Parot, Y., Pérez, R., Pheav, D., Picot, L., Pilleri, P., Pilorget, C., Pinet, P., Pont, G., Poulet, F., Quantin-Nataf, C., Quertier, B., Rambaud, D., Rapin, W., Romano, P., Roucayrol, L., Royer, C., Ruellan, M., Sandoval, B.F., Sautter, V., Schoppers, M.J., Schröder, S., Seran, H.-C., Sharma, S.K., Sobron, P., Sodki, M., Sournac, A., Sridhar, V., Standarovsky, D., Storms, S., Striebig, N., Tatat, M., Toplis, M., Torre-Fdez, I., Toulemont, N., Velasco, C., Veneranda, M., Venhaus, D., Virmontois, C., Viso, M., Willis, P., Wong, K.W., 2021. The SuperCam instrument suite on the Mars 2020 rover: science objectives and mast-unit description. Space Sci. Rev. 217, 47.

Mandon, L., Quantin-Nataf, C., Thollot, P., Mangold, N., Lozac'h, L., Dromart, G., Beck, P., Dehouck, E., Breton, S., Millot, C., Volat, M., 2020. Refining the age, emplacement and alteration scenarios of the olivine-rich unit in the Nili Fossae region, Mars. Icarus 336, 113436.

Meslin, P.-Y., et al.. Diversity and Areal Density of Iron-Nickel Meteorites Analyzed by Chemcam in Gale Crater. https://ui.adsabs.harvard.edu/abs/2019LPI….50.3179M.

Mezzacappa, A., Melikechi, N., Cousin, A., Lasue, J., Lanza, N., Wiens, R.C., Clegg, S.M., Maurice, S., Bender, S., Berger, G., Forni, O., Gasnault, O., Newsom, H., Ollila, A.M., Clark, B., Dyar, M.D., Blaney, D., Team, M.S., 2014. Effects of distance correction on ChemCam LIBS measurements (sols 13 to 360). In: 45th Annual Lunar and Planetary Science Conference, p. 1517.

Millour, E., Forget, F., Spiga, A., Vals, M., Zakharov, V., Montabone, L., Lefèvre, F., Montmessin, F., Chaufray, J.-Y., López-Valverde, M.A., González-Galindo, F., Lewis, S.R., Read, P.L., Desjean, M.-C., Cipriani, F., Team, M.D., 2018. The Mars climate database (version 5.3). In: From Mars Express to ExoMars, p. 68.

Moroz, L.V., Basilevsky, A.T., Hiroi, T., Rout, S.S., Baither, D., van der Bogert, C.H., Yakovlev, O.I., Fisenko, A.V., Semjonova, L.F., Rusakov, V.S., Khramov, D.A., Zinovieva, N.G., Arnold, G., Pieters, C.M., 2009. Spectral properties of simulated impact glasses produced from martian soil analogue JSC Mars-1. Icarus 202, 336–353.

Morris, R.V., Ruff, S.W., Gellert, R., Ming, D.W., Arvidson, R.E., Clark, B.C., Golden, D.C., Siebach, K., Klingelhöfer, G., Schröder, C., Fleischer, I., Yen, A.S., Squyres, S.W., 2010. Identification of carbonate-rich outcrops on mars by the Spirit Rover. Science 329, 421.

Mumma, M.J., Villanueva, G.L., Novak, R.E., Hewagama, T., Bonev, B.P., DiSanti, M.A., Mandell, A.M., Smith, M.D., 2009. Strong release of methane on mars in Northern Summer 2003. Science 323, 1041.

Nachon, M., Clegg, S.M., Mangold, N., Schröder, S., Kah, L.C., Dromart, G., Ollila, A., Johnson, J.R., Oehler, D.Z., Bridges, J.C., Le Mouélic, S., Forni, O., Wiens, R.C., Anderson, R.B., Blaney, D.L., Bell, J.F., Clark, B., Cousin, A., Dyar, M.D., Ehlmann, B., Fabre, C., Gasnault, O., Grotzinger, J., Lasue, J., Lewin, E., Léveillé, R., McLennan, S., Maurice, S., Meslin, P.-Y., Rapin, W., Rice, M., Squyres, S.W., Stack, K., Sumner, D.Y., Vaniman, D., Wellington, D., 2014. Calcium sulfate veins characterized by ChemCam/Curiosity at Gale crater, Mars. J. Geophys. Res. (Planets) 119, 1991–2016.

Ollila, A.M., Blank, J.G., Wiens, R.C., Lasue, J., Newsom, H.E., Clegg, S.M., Cousin, A., Maurice, S., 2011. Preliminary results on the capabilities of the ChemCam laser-induced breakdown spectroscopy (LIBS) instrument to detect carbon on Mars. In: 42nd Annual Lunar and Planetary Science Conference, p. 2395.

Ollila, A.M., Newsom, H.E., Wiens, R.C., Lasue, J., Clegg, S.M., Cousin, A., Gasnault, O., Forni, O., Maurice, S., Schroeder, S., Meslin, P.-Y., Dyar, M.D., Blank, J.G., Clark, B., Barraclough, B., Team, M.S.L., 2013. Early results from Gale crater on ChemCam detections of carbon, Lithium, and rubidium. In: 44th Annual Lunar and Planetary Science Conference, p. 2188.

Phan, V.T.H., Quirico, E., Beck, P., Le Brech, Y., Jovanovic, L., Le Guillou, C., Bernard, S., Bonal, L., Carrasco, N., Gautier, T., Raya, J., 2021. Infrared spectroscopy quantification of functional carbon groups in kerogens and coals: A calibration procedure. Spectrochim. Acta A Mol. Biomol. Spectrosc. 259, 119853 https://doi.org/10.1016/j.saa.2021.119853.

Quirico, E., Bonal, L., 2019. Organic matter in interplanetary dusts and meteorites. Adv. Astrobiol. Biogeophys. https://doi.org/10.1007/978-3-319-96175-0_2.

Quirico, E., Moroz, L.V., Schmitt, B., Arnold, G., Faure, M., Beck, P., Bonal, L., Ciarniello, M., Capaccioni, F., Filacchione, G., Erard, S., Leyrat, C., Bockelée-Morvan, D., Zinzi, A., Palomba, E., Drossart, P., Tosi, F., Capria, M.T., De Sanctis, M. C., Raponi, A., Fonti, S., Mancarella, F., Orofino, V., Barucci, A., Blecka, M.I., Carlson, R., Despan, D., Faure, A., Fornasier, S., Gudipati, M.S., Longobardo, A., Markus, K., Mennella, V., Merlin, F., Piccioni, G., Rousseau, B., Taylor, F., 2016. Refractory and semi-volatile organics at the surface of comet 67P/Churyumov-Gerasimenko: insights from the VIRTIS/Rosetta imaging spectrometer. Icarus 272, 32–47. https://doi.org/10.1016/j.icarus.2016.02.028.

Rampe, E.B., Bristow, T.F., Morris, R.V., Morrison, S.M., Achilles, C.N., Ming, D.W., Vaniman, D.T., Blake, D.F., Tu, V.M., Chipera, S.J., Yen, A.S., Peretyazhko, T.S., Downs, R.T., Hazen, R.M., Treiman, A.H., Grotzinger, J.P., Castle, N., Craig, P.I., Des Marais, D.J., Thorpe, M.T., Walroth, R.C., Downs, G.W., Fraeman, A.A., Siebach, K. L., Gellert, R., Lafuente, B., McAdam, A.C., Meslin, P.-Y., Sutter, B., Salvatore, M.R., 2020. Mineralogy of Vera Rubin ridge from the Mars science laboratory CheMin instrument. J. Geophys. Res. (Planets) 125, e06306.

Rapin, W., 2016. Hydratation de la surface de Mars par les données du rover Curiosity. Thèse de l'Université de Toulouse III, Paul Sabatier.

Rapin, W., Meslin, P.-Y., Maurice, S., Vaniman, D., Nachon, M., Mangold, N., Schröder, S., Gasnault, O., Forni, O., Wiens, R.C., Martínez, G.M., Cousin, A., Sautter, V., Lasue, J., Rampe, E.B., Archer, D., 2016. Hydration state of calcium sulfates in Gale crater, Mars: identification of bassanite veins. Earth Planet. Sci. Lett. 452, 197–205. https://doi.org/10.1016/j.epsl.2016.07.045.

Rapin, W., Meslin, P.-Y., Maurice, S., Wiens, R.C., Laporte, D., Chauviré, B., Gasnault, O., Schröder, S., Beck, P., Bender, S., Beyssac, O., Cousin, A., Dehouck, E., Drouet, C., Forni, O., Nachon, M., Melikechi, N., Rondeau, B., Mangold, N., Thomas, N.H., 2017. Quantification of water content by laser induced breakdown spectroscopy on Mars. Spectrochimica Acta - Part B Atomic Spectrosc. 130, 82–100. https://doi.org/10.1016/j.sab.2017.02.007.

Rapin, W., Ehlmann, B.L., Dromart, G., Schieber, J., Thomas, N.H., Fischer, W.W., Fox, V. K., Stein, N.T., Nachon, M., Clark, B.C., Kah, L.C., Thompson, L., Meyer, H.A., Gabriel, T.S.J., Hardgrove, C., Mangold, N., Rivera-Hernandez, F., Wiens, R.C., Vasavada, A.R., 2019. An interval of high salinity in ancient Gale crater lake on Mars. Nat. Geosci. 12, 889–895. https://doi.org/10.1038/s41561-019-0458-8.

Ruff, S.W., Hamilton, V.E., Rogers, A.D., Edwards, C.S., Horgan, B.H.N., 2022. Olivine and carbonate-rich bedrock in Gusev crater and the Nili Fossae region of Mars may be altered ignimbrite deposits. Icarus 380, 114974.

Scheller, E.L., Swindle, C., Grotzinger, J., Barnhart, H., Bhattacharjee, S., Ehlmann, B.L., Farley, K., Fischer, W.W., Greenberger, R., Ingalls, M., Martin, P.E., Osorio-Rodriguez, D., Smith, B.P., 2021. Formation of Magnesium Carbonates on Earth and Implications for Mars. Journal of Geophysical Research (Planets) 126, e06828.

Schröder, S., Rammelkamp, K., Vogt, D.S., Gasnault, O., Hübers, H.-W., 2019. Contribution of a martian atmosphere to laser-induced breakdown spectroscopy (LIBS) data and testing its emission characteristics for normalization applications. Icarus 325, 1–15. https://doi.org/10.1016/j.icarus.2019.02.017.

Schwartz, S., 2000. La zone piémontaise des Alpes occidentales : un paléocomplexe de subduction. Arguments métamorphiques, géochronologiques et structuraux. Thèse Université Claude Bernard, Lyon.

Steininger, H., Goesmann, F., Goetz, W., 2012. Influence of magnesium perchlorate on the pyrolysis of organic compounds in Mars analogue soils. Planet. Space Sci. 71, 9–17. https://doi.org/10.1016/j.pss.2012.06.015.

Stern, J.C., et al., 2015. Evidence for indigenous nitrogen in sedimentary and aeolian deposits from the Curiosity rover investigations at Gale crater, Mars. Proceed. National Acad. Sci. 112, 4245–4250.

Stern, J.C., et al., 2018. Major Volatiles Evolved From Eolian Materials in Gale Crater. Geophys. Res. Lett. 45, 10240–10248.

Stern, J.C., Malespin, C.A., Eigenbrode, J.L., Webster, C.R., Flesch, G., Franz, H.B., Graham, H.V., House, C.H., Sutter, B., Archer, P.D., Hofmann, A.E., McAdam, A.C., Ming, D.W., Navarro-Gonzalez, R., Steele, A., Freissinet, C., Mahaffy, P.R., 2022. Organic carbon concentrations in 3.5-billion-year-old lacustrine mudstones of Mars. In: Proceedings of the National Academy of Science.

Stern, J.C., Sutter, B., Jackson, W.A., Navarro-González, R., McKay, C.P., Ming, D.W., Archer, P.D., Mahaffy, P.R., 2017. The nitrate/(per)chlorate relationship on Mars. Geophy. Res. Let. 44, 2643–2651.

Sutter, B., McAdam, A.C., Mahaffy, P.R., Ming, D.W., Edgett, K.S., Rampe, E.B., Eigenbrode, J.L., Franz, H.B., Freissinet, C., Grotzinger, J.P., Steele, A., House, C.H., Archer, P.D., Malespin, C.A., Navarro-González, R., Stern, J.C., Bell, J.F., Calef, F.J., Gellert, R., Glavin, D.P., Thompson, L.M., Yen, A.S., 2017. Evolved gas analyses of sedimentary rocks and eolian sediment in Gale crater, Mars: results of the curiosity rover's sample analysis at Mars instrument from Yellowknife Bay to the Namib dune. J. Geophys. Res. (Planets) 122, 2574–2609.

Szopa, C., Freissinet, C., Glavin, D.P., Millan, M., Buch, A., Franz, H.B., Summons, R.E., Sumner, D.Y., Sutter, B., Eigenbrode, J.L., Williams, R.H., Navarro-González, R., Guzman, M., Malespin, C., Teinturier, S., Mahaffy, P.R., Cabane, M., 2020. First detections of dichlorobenzene isomers and trichloromethylpropane from organic matter indigenous to mars mudstone in Gale Crater, Mars: results from the sample analysis at mars instrument onboard the curiosity rover. Astrobiology 20, 292–306.

Thorpe, M.T., Bristow, T.F., Rampe, E.B., Tosca, N.J., Grotzinger, J.P., Bennett, K.A., Achilles, C.N., Blake, D.F., Chipera, S.J., Downs, G., Downs, R.T., Morrison, S.M., Tu, V., Castle, N., Craig, P., Marais, D.J.D., Hazen, R.M., Ming, D.W., Morris, R.V., Treiman, A.H., Vaniman, D.T., Yen, A.S., Vasavada, A.R., Dehouck, E., Bridges, J.C., Berger, J., McAdam, A., Peretyazhko, T., Siebach, K.L., Bryk, A.B., Fox, V.K., Fedo, C. M., 2022. Mars science laboratory CheMin data from the Glen Torridon region and the significance of lake-groundwater interactions in interpreting mineralogy and sedimentary history. J. Geophys. Res. (Planets) 127 e2021JE007099.

Vaniman, D., Dyar, M.D., Wiens, R., Ollila, A., Lanza, N., Lasue, J., Rhodes, J.M., Clegg, S., Newsom, H., 2012. Ceramic ChemCam calibration targets on Mars science laboratory. Space Sci. Rev. 170, 229–255. https://doi.org/10.1007/s11214-012-9886-0.

Vogt, D.S., Schröder, S., Frohmann, S., Hansen, P.B., Seel, F., Gensch, M., Hübers, H.-W., 2022. Spatiotemporal characterization of the laser-induced plasma plume in simulated Martian conditions. Spectrochim. Acta B At. Spectrosc. 187, 106326 https://doi.org/10.1016/j.sab.2021.106326.

Webster, C.R., Mahaffy, P.R., Atreya, S.K., Flesch, G.J., Mischna, M.A., Meslin, P.-Y., Farley, K.A., Conrad, P.G., Christensen, L.E., Pavlov, A.A., Martín-Torres, J., Zorzano, M.-P., McConnochie, T.H., Owen, T., Eigenbrode, J.L., Glavin, D.P., Steele, A., Malespin, C.A., Archer, P. Douglas, Sutter, B., Coll, P., Freissinet, C., McKay, C.P., Moores, J.E., Schwenzer, S.P., Bridges, J.C., Navarro-Gonzalez, R., Gellert, R., Lemmon, M.T., Team, M.S., Abbey, W., Achilles, C., Agard, C., Alexandre Alves Verdasca, J., Anderson, J., Anderson, R.C., Anderson, R.B., Appel, J.K., Archer, Paul Douglas, Arevalo, R., Armiens-Aparicio, C., Arvidson, R., Atlaskin, E., Atreya, A.S., Azeez, A.S., Baker, B., Baker, M., Balic-Zunic, T., Baratoux, D., Baroukh, J., Barraclough, B., Battalio, M., Beach, M., Bean, K., Beck, P., Becker, R., Beegle, L., Behar, A., Belgacem, I., Bell, J.F., Bender, S., Benna, M., Bentz, J., Berger, J., Berger, T., Berlanga, G., Berman, D., Bish, D., Blacksberg, J., Blake, D.F., José Blanco, J., Blaney, Á.D., Blank, J., Blau, H., Bleacher, L., Boehm, E., Bonnet, J.-Y., Botta, O., Böttcher, S., Boucher, T., Bower, H., Boyd, N., Boynton, W., Braswell, S., Breves, E., Bridges, J.C., Bridges, N., Brinckerhoff, W., Brinza, D., Bristow, T., Brunet, C., Brunner, A., Brunner, W., Buch, A., Bullock, M., Burmeister, S., Burton, J., Buz, J., Cabane, M., Calef, F., Cameron, J., Campbell, J.L., Cantor, B., Caplinger, M., Clifton, C., Caride Rodríguez, J., Carmosino, M., Carrasco Blázquez, I., Cavanagh, P., Charpentier, A., Chipera, S., Choi, D., Christensen, L., Clark, B., Clegg, S., Cleghorn, T., Cloutis, E., Cody, G., Coll, P., Coman, E.I., Conrad, P., Coscia, D., Cousin, A., Cremers, D., Crisp, J.A., Cropper, K., Cros, A., Cucinotta, F., d'Uston, C., Davis, S., Day, M., Daydou, Y., DeFlores, L., Dehouck, E., Delapp, D., DeMarines, J., Dequaire, T., Des Marais, D., Desrousseaux, R., Dietrich, W., Dingler, R., Domagal-Goldman, S., Donny, C., Downs, R., Drake, D., Dromart, G., Dupont, A., Duston, B., Dworkin, J.P., Dyar, M.D., Edgar, L., Edgett, K., Edwards, C.S., Edwards, L., Edwards, P., Ehlmann, B., Ehresmann, B., Eigenbrode, J., Elliott, B., Elliott, H., Ewing, R., Fabre, C., Fairén, A., Fairén, A., Farley, K., Farmer, J., Fassett, C., Favot, L., Fay, D., Fedosov, F., Feldman, J., Fendrich, K., Fischer, E., Fisk, M., Fitzgibbon, M., Flesch, G., Floyd, M., Flückiger, L., Forni, O., Fox, V., Fraeman, A., Francis, R., François, P., Franz, H., Freissinet, C., French, K.L., Frydenvang, J., Garvin, J., Gasnault, O., Geffroy, C., Gellert, R., Genzer, M., Getty, S., Glavin, D., Godber, A., Goesmann, F., Goetz, W., Golovin, D., Gómez Gómez, F., Gómez-Elvira, J., Gondet, B., Gordon, S., Gorevan, S., Graham, H., Grant, J., Grinspoon, D., Grotzinger, J., Guillemot, P., Guo, J., Gupta, S., Guzewich, S., Haberle, R., Halleaux, D., Hallet, B., Hamilton, V., Hand, K., Hardgrove, C., Hardy, K., Harker, D., Harpold, D., Harri, A.-M., Harshman, K., Hassler, D., Haukka, H., Hayes, A., Herkenhoff, K., Herrera, P., Hettrich, S., Heydari, E., Hipkin, V., Hoehler, T., Hollingsworth, J., Hudgins, J., Huntress, W., Hurowitz, J., Hviid, S., Iagnemma, K., Indyk, S., Israël, G., Jackson, R.S., Jacob, S., Jakosky, B., Jean-Rigaud, L., Jensen, E., Kløvgaard Jensen, J., Johnson, J.R., Johnson, M., Johnstone, S., Jones, A., Jones, J.H., Joseph, J., Joulin, M., Jun, I., Kah, L.C., Kahanpää, H., Kahre, M., Kaplan, H., Karpushkina, N., Kashyap, S., Kauhanen, J., Keely, L., Kelley, S., Kempe, F., Kemppinen, O., Kennedy, M.R., Keymeulen, D., Kharytonov, A., Kim, M.-H, Kinch, K., King, P., Kirk, R., Kirkland, L., Kloos, J., Kocurek, G., Koefoed, A., Köhler, J., Kortmann, O., Kotrc, B., Kozyrev, A., Krau, J., Krezoski, B.G., Kronyak, R., Krysak, D., Kuzmin, R., Lacour, J.-L., Lafaille, V., Langevin, Y., Lanza, N., Lapôtre, M., Larif, M.-F., Lasue, J., Le Deit, L., Le Mouélic, S., Lee, E.M., Lee, Q.-M., Lee, R., Lees, D., Lefavor, M., Lemmon, M., Lepinette, A., Lepore, M.K., Leshin, L., Léveillé, R., Lewin, É., Lewis, K., Li, S., Lichtenberg, K., Lipkaman, L., Lisov, D., Little, C., Litvak, M., Liu, C., Lohf, H., Lorigny, E., Lugmair, G., Lundberg, A., Lyness, E., Madsen, M.B., Magee, A., Mahaffy, P., Maki, J., Mäkinen, T., Malakhov, A., Malespin, C., Malin, M., Mangold, N., Manhes, G., Manning, H., Marchand, G., Marín García, C., Marín Jiménez, M., Martín García, C., Martin, D.K., Martin, M., Martin, P., Martínez Martínez, G., Martínez-Frías, J., Martín-Sauceda, J., Martín-Soler, M.J., Martín-Torres, F.J., Mason, E., Matthews, T., Matthiä, D., Mauchien, P., Maurice, S., McAdam, A., McBride, M., McCartney, E., McConnochie, T., McCullough, E., McEwan, I., McKay, C., McLain, H., McLennan, S., McNair, S., Melikechi, N., Mendaza de Cal, T., Merikallio, S., Merritt, S., Meslin, P.-Y., Meyer, M., Mezzacappa, A., Milkovich, S., Millan, M., Miller, H., Miller, K., Milliken, R., Ming, D., Minitti, M., Mischna, M., Mitchell, J., Mitrofanov, I., Moersch, J., Mokrousov, M., Molina, A., Moore, J.C., Moores, J.E., Mora-Sotomayor, L., Moreno, G., Morookian, J.M., Morris, R.V., Morrison, S., Mousset, V.,

Mrigakshi, A., Mueller-Mellin, R., Muller, J.-P., Muñoz Caro, G., Nachon, M., Nastan, A., Navarro López, S., Navarro González, R., Nealson, K., Nefian, A., Nelson, T., Newcombe, M., Newman, C., Newsom, H., Nikiforov, S., Nikitczuk, M., Niles, P., Nixon, B., Noblet, A., Noe, E., Nolan, D.T., Oehler, D., Ollila, A., Olson, T., Orthen, T., Owen, T., Ozanne, M., de Pablo Hernández, M.Á., Pagel, H., Paillet, A., Pallier, E., Palucis, M., Parker, T., Parot, Y., Parra, A., Patel, M., Paton, M., Paulsen, G., Pavlov, A., Pavri, B., Peinado-González, V., Pepin, R., Peret, L., Pérez, R., Perrett, G., Peterson, J., Pilorget, C., Pinet, P., Pinnick, V., Pla-García, J., Plante, I., Poitrasson, F., Polkko, J., Popa, R., Posiolova, L., Posner, A., Pradler, I., Prats, B., Prokhorov, V., Raaen, E., Radziemski, L., Rafkin, S., Ramos, M., Rampe, E., Rapin, W., Raulin, F., Ravine, M., Reitz, G., Ren, J., Rennó, N., Rice, M., Richardson, M., Ritter, B., Rivera-Hernández, F., Robert, F., Robertson, K., Rodriguez Manfredi, J.A., José Romeral-Planelló, J., Rowland, S., Rubin, D., Saccoccio, M., Said, D., Salamon, A., Sanin, A., Sans Fuentes, S.A., Saper, L., Sarrazin, P., Sautter, V., Savijärvi, H., Schieber, J., Schmidt, M., Schmidt, W., Scholes, D., Schoppers, M., Schröder, S., Schwenzer, S.P., Sciascia Borlina, C., Scodary, A., Sebastián Martínez, E., Sengstacken, A., Shechet, J.G., Shterts, R., Siebach, K., Siili, T., Simmonds, J.J., Sirven, J.-B., Slavney, S., Sletten, R., Smith, M.D., Sobron Sanchez, P., Spanovich, N., Spray, J., Spring, J., Squyres, J., Stack, K., Stalport, F., Starr, R., Stein, A.S.T., Stern, J., Stewart, N., Stewart, W., Stipp, S.S.L., Stoiber, K., Stolper, E., Sucharski, R., Sullivan, R., Summons, R., Sumner, D.Y., Sun, V., Supulver, K., Sutter, B., Szopa, C., Tan, F., Tate, C., Teinturier, S., ten Kate, I.L., Thomas, A., Thomas, P., Thompson, L., Thuillier, F., Thulliez, E., Tokar, R., Toplis, M., de la Torre Juárez, M., Torres Redondo, J., Trainer, M., Treiman, A., Tretyakov, V., Ullán-Nieto, A., Urqui-O'Callaghan, R., Valentín-Serrano, P., Van Beek, J., Van Beek, T., VanBommel, S., Vaniman, D., Varenikov, A., Vasavada, A.R., Vasconcelos, P., de Vicente-Retortillo Rubalcaba, Á., Vicenzi, E., Vostrukhin, A., Voytek, M., Wadhwa, M., Ward, J., Watkins, J., Webster, C.R., Weigle, G., Wellington, D., Westall, F., Wiens, R., Wilhelm, M.B., Williams, A., Williams, J., Williams, R., Williams, R.B., Williford, K., Wilson, M.A., Wilson, S.A., Wimmer-Schweingruber, R., Wolff, M., Wong, M., Wray, J., Yana, C., Yen, A., Yingst, A., Zeitlin, C., Zimdar, R., Zorzano Mier, M.-P., 2015. Mars methane detection and variability at Gale crater. Science 347, 415-417.

Webster, C.R., Mahaffy, P.R., Atreya, S.K., Moores, J.E., Flesch, G.J., Malespin, C., McKay, C.P., Martinez, G., Smith, C.L., Martin-Torres, J., Gomez-Elvira, J., Zorzano, M.-P., Wong, M.H., Trainer, M.G., Steele, A., Archer, D., Sutter, B., Coll, P. J., Freissinet, C., Meslin, P.-Y., Gough, R.V., House, C.H., Pavlov, A., Eigenbrode, J. L., Glavin, D.P., Pearson, J.C., Keymeulen, D., Christensen, L.E., Schwenzer, S.P., Navarro-Gonzalez, R., Pla-García, J., Rafkin, S.C.R., Vicente-Retortillo, Á., Kahanpää, H., Viudez-Moreiras, D., Smith, M.D., Harri, A.-M., Genzer, M., Hassler, D.M., Lemmon, M., Crisp, J., Sander, S.P., Zurek, R.W., Vasavada, A.R., 2018. Background levels of methane in Mars' atmosphere show strong seasonal variations. Science 360, 1093–1096.

Webster, C.R., Mahaffy, P.R., Pla-Garcia, J., Rafkin, S.C.R., Moores, J.E., Atreya, S.K., Flesch, G.J., Malespin, C.A., Teinturier, S.M., Kalucha, H., Smith, C.L., Viúdez-Moreiras, D., Vasavada, A.R., 2021. Day-night differences in Mars methane suggest nighttime containment at Gale crater. Astronomy (Astrophysics) 650, A166.

Wiens, R.C., et al., 2021. The SuperCam Instrument Suite on the NASA Mars 2020 Rover: Body Unit and Combined System Tests. Space Science Reviews 217, 4.

Wiens, R.C., Maurice, S., Barraclough, B., Saccoccio, M., Barkley, W.C., Bell III, J.F., Bender, S., Bernardin, J., Blaney, D., Blank, J., Bouyé, M., Bridges, N., Bultman, N., Caïs, P., Clanton, R.C., Clark, B., Clegg, S., Cousin, A., Cremers, D., Cros, A., Deflores, L., Delapp, D., Dingler, R., D'Uston, C., Darby Dyar, M., Elliott, T., Enemark, D., Fabre, C., Flores, M., Forni, O., Gasnault, O., Hale, T., Hays, C., Herkenhoff, K., Kan, E., Kirkland, L., Kouach, D., Landis, D., Langevin, Y., Lanza, N., Larocca, F., Lasue, J., Latino, J., Limonadi, D., Lindensmith, C., Little, C., Mangold, N., Manhes, G., Mauchien, P., McKay, C., Miller, E., Mooney, J., Morris, R. V., Morrison, L., Nelson, T., Newsom, H., Ollila, A., Ott, M., Pares, R., Perez, R., Poitrasson, F., Provost, C., Reiter, J.W., Roberts, T., Romero, F., Sautter, V., Salazar, S., Simmonds, J.J., Stiglich, R., Storms, S., Striebig, N., Thocaven, J.-J., Trujillo, T., Ulibarri, M., Vaniman, D., Warner, N., Waterbury, R., Whitaker, R., Witt, J., Wong-Swanson, B., 2012. The ChemCam instrument suite on the Mars science laboratory (MSL) rover: body unit and combined system tests. Space Sci. Rev. 170, 167–227. https://doi.org/10.1007/s11214-012-9902-4.

Wiens, R.C., Maurice, S., Lasue, J., Forni, O., Anderson, R.B., Clegg, S., Bender, S., Blaney, D., Barraclough, B.L., Cousin, A., Deflores, L., Delapp, D., Dyar, M.D., Fabre, C., Gasnault, O., Lanza, N., Mazoyer, J., Melikechi, N., Meslin, P.-Y., Newsom, H., Ollila, A., Perez, R., Tokar, R.L., Vaniman, D., 2013. Pre-flight calibration and initial data processing for the ChemCam laser-induced breakdown spectroscopy instrument on the Mars science laboratory rover. Spectrochimica Acta - Part B Atomic Spectrosc. 82, 1–27. https://doi.org/10.1016/j.sab.2013.02.003.

Wiens, R.C., Udry, A., Beyssac, O., Quantin-Nataf, C., Mangold, N., Cousin, A., Mandon, L., Bosak, T., Forni, O., McLennan, S.M., Sautter, V., Brown, A., Benzerara, K., Johnson, J.R., Mayhew, L., Maurice, S., Anderson, R.B., Clegg, S.M., Crumpler, L., Gabriel, T.S.J., Gasda, P., Hall, J., Horgan, B.H.N., Kah, L., Legett, C., Madariaga, J.M., Meslin, P.-Y., Ollila, A.M., Poulet, F., Royer, C., Sharma, S.K., Siljeström, S., Simon, J.I., Acosta-Maeda, T.E., Alvarez-Llamas, C., Angel, S.M., Arana, G., Beck, P., Bernard, S., Bertrand, T., Bousquet, B., Castro, K., Chide, B., Clavé, E., Cloutis, E., Connell, S., Dehouck, E., Dromart, G., Fischer, W., Fouchet, T., Francis, R., Frydenvang, J., Gasnault, O., Gibbons, E., Gupta, S., Hausrath, E.M., Jacob, X., Kalucha, H., Kelly, E., Knutsen, E., Lanza, N., Laserna, J., Lasue, J., Le Mouélic, S., Leveille, R., Lopez Reyes, G., Lorenz, D., Manrique, J.A., Martinez-Frias, J., McConnochie, T., Melikechi, N., Mimoun, D., Montmessin, F., Moros, J., Murdoch, N., Pilleri, P., Pilorget, C., Pinet, P., Rapin, W., Rull, F., Schröder, S., Shuster, D.L., Smith, R.J., Stott, A.E., Tarnas, J., Turenne, N., Veneranda, M., Vogt, D.S., Weiss, B.P., Willis, P., Stack, K.M., Williford, K.H., Farley, K.A., 2022. Compositionally and density stratified igneous terrain in Jezero crater, Mars. Sci 8, eabo3399.

Yang, F., Li, L.-N., Xu, W.-M., Liu, X.-F., Cui, Z.-C., Jia, L.-C., Liu, Y., Xu, J.-H., Chen, Y.-W., Xu, X.-S., Wang, J.-Y., Qi, H., Shu, R., 2022. Laser-induced breakdown spectroscopy combined with a convolutional neural network: A promising methodology for geochemical sample identification in Tianwen-1 Mars mission. Spectrochim. Acta B At. Spectrosc. 192, 106417 https://doi.org/10.1016/j.sab.2022.106417.